Activation of naïve CD4$^+$ T cells re-tunes STAT1 signaling to deliver unique cytokine responses in memory CD4$^+$ T cells

Jason P. Twohig[1,2#], Ana Cardus Figueras[1,2#], Robert Andrews[2], Florian Wiede[3,4], Benjamin C. Cossins[1,2], Alicia Derrac Soria[1,2], Myles J. Lewis[5], Michael J. Townsend[6], David Millrine[1,2], Jasmine Li[3,7], David G. Hill[1,2], Javier Uceda Fernandez[1,2,∞], Xiao Liu[1,2], Barbara Szomolay[1,2], Christopher J. Pepper[8,9], Philip R. Taylor[1,2], Costantino Pitzalis[5], Tony Tiganis[3,4], Nigel M. Williams[10], Gareth W. Jones[1,2,11] & Simon A. Jones[1,2*]

Affiliations:

1. Division of Infection & Immunity, School of Medicine, Cardiff University, Cardiff, Wales, UK
2. Systems Immunity University Research Institute, Cardiff University, Cardiff, Wales, UK
3. Monash Biomedicine Discovery Institute, Monash University, Clayton, Victoria 3800, Australia
4. Department of Biochemistry and Molecular Biology, Monash University, Clayton, Victoria 3800, Australia
5. Centre for Experimental Medicine & Rheumatology, William Harvey research Institute, Queen Mary's School of Medicine & Dentistry, London, UK
6. ITGR Diagnostics Discovery, Genentech Research & Early Development, 1 DNA Way, South San Francisco, CA94080, USA
7. Department of Microbiology, Monash University, Clayton, Victoria 3800, Australia
8. Division of Cancer & Genetics, School of Medicine, Cardiff University, Cardiff, Wales, UK
9. Brighton and Sussex Medical School, University of Sussex, Brighton, UK
10. Division of Psychological Medicine & Clinical Neuroscience, School of Medicine, Cardiff University, Cardiff, Wales, UK.
11. School of Cellular and Molecular Medicine, Biomedical Sciences Building, University Walk, University of Bristol, Bristol, UK

[#]JPT and ACF contributed equally to the manuscript; [∞]JUF deceased 29th August 2018.

[*]**Corresponding author:**

Professor Simon A. Jones,

Division of Infection and Immunity, School of Medicine, Cardiff University, Heath Park, Cardiff, CF14 4XN, Wales, UK.

Tel: +44 29 2068 7325; Fax: +44 29 2068 7303; E-mail: JonesSA@cf.ac.uk

ABSTRACT

The cytokine IL-6 controls the survival, proliferation and effector characteristics of lymphocytes through activation of the transcription factors STAT1 and STAT3. While STAT3 activity is an ever-present feature of IL-6 signaling in $CD4^+$ T cells, prior T-cell receptor activation limits the IL-6 control of STAT1 in effector and memory populations. Here we show that STAT1 phosphorylation in response to IL-6 was regulated by protein tyrosine phosphatases (PTPN2, PTPN22) expressed in response to the activation of naïve $CD4^+$ T cells. Transcriptomic and chromatin immunoprecipitation-sequencing of IL-6 responses in naïve and effector memory $CD4^+$ T cells showed how the suppression of STAT1 activation shaped the functional identity and effector characteristics of memory $CD4^+$ T cells. Thus, protein tyrosine phosphatases induced by activation of naïve T cells determined the way activated or memory $CD4^+$ T cells sensed and interpreted cytokine signals.

Naïve, activated and memory T cells display differences in their ability to respond to antigen. These include changes in proliferation, survival, sensitivity to antigen, dependence on co-stimulatory signals and alterations in T cell homing[1]. Cytokines responsible for the control of these activities often signal through receptor-associated Janus kinases (Jak proteins) that regulate cytoplasmic transcription factors termed signal transducers and activators of transcription (STAT)[2]. Thus, the Jak-STAT pathway senses and interprets environmental signals essential for proliferation and functional identity[2]. Here, we examined whether cytokine cues delivered by the Jak-STAT pathway can be adapted to fine-tune the effector properties of individual $CD4^+$ T cell subsets.

Studies of infection, inflammation, autoimmunity and cancer demonstrate that the cytokine IL-6 is essential for the generation of adaptive immunity[3]. Activities include the maturation and maintenance of antibody secreting B cells, and responses that shape the effector characteristics of $CD4^+$ T helper (T_H) cells[3]. In this regard, mice lacking IL-6 often show deficiencies in T cell effector function and memory recall[4, 5, 6, 7, 8, 9]. Studies also suggest that $CD4^+$ T cells display differences in IL-6 responsiveness that may reflect the activation status of the T cell[7, 10, 11, 12]. How these differences arise is currently unclear.

The receptor complex responsible for IL-6 signaling consists of a type-1 cytokine receptor (IL-6R, CD126) and a signal-transducing β-receptor (gp130, CD130) subunit[3]. IL-6R is shed in response to $CD4^+$ T cell activation, and inflammatory T cells from sites of disease often display low IL-6R expression[7, 10, 12, 13, 14, 15, 16, 17]. IL-6 activates the latent transcription factors STAT1 and STAT3[3]. IL-6 control of STAT3 is essential for T cell recruitment and survival and the maintenance of activated T cells within inflamed tissues[11, 14, 16]. These STAT3-driven responses include the transactivation of anti-apoptotic regulators and genes that determine the effector or regulatory characteristic of $CD4^+$ T cells[3, 11, 18]. In contrast, IL-6 activation of STAT1 plays a more regulatory role and often determines the transcriptional output of STAT3[18, 19, 20, 21]. These studies illustrate a complex interplay between STAT1 and STAT3, and emphasize how STAT1 signaling may shape the biological properties of IL-6[18, 20, 21, 22, 23, 24]. Significantly, $CD4^+$ T cell activation has been shown to alter IL-6 signaling through STAT1[9, 11]. Here we show that STAT1 phosphorylation in response to IL-6 is suppressed in activated and memory $CD4^+$ T cells and identified protein tyrosine phosphatases as regulators of STAT1 activity. Our data further showed how this re-programming mechanism may influence the way effector memory $CD4^+$ T cells sense and interpret IL-6 signals in disease.

RESULTS

Infiltrating synovial CD4$^+$ T cells have altered IL-6-mediated STAT1 activation

Previous studies suggest that CD4$^+$ T cell activation alters cytokine signaling through the Jak-STAT pathway[4, 9, 11]. To further these findings we established antigen-induced arthritis (AIA) in C57Bl/6 wild-type mice through immunization with methylated BSA (mBSA). Histological joint sections from day 10 of AIA were evaluated for tyrosine phosphorylated STAT1 and STAT3 (hereafter pY-STAT1 and pY-STAT3) using immunofluorescence (Fig. 1a). While pY-STAT3 co-localized with CD3$^+$ T cells, pY-STAT1 showed weak co-localization with the CD3 stain (Fig. 1a). To verify these observations, CD4$^+$ T cells were isolated at day 10 of AIA from the inflamed synovium of wild-type mice and stimulated *ex vivo* with IL-6 (20ng/ml). When compared to IL-6-treated CD4$^+$CD25$^-$CD44^{lo}CD62L^{hi}CD127^{hi} naïve T cells (T_N cells) from the spleen of wild-type mice, intracellular flow cytometry showed that synovial CD4$^+$ T cells displayed reduced pY-STAT1 staining (Fig. 1b). Both CD4$^+$ T cell populations displayed comparable pY-STAT3 responses to IL-6 (Fig. 1b). To test whether prior antigenic challenge with mBSA restricted the ability of IL-6 to signal through STAT1, we extracted total CD4$^+$ T cells from the inguinal draining lymph nodes of wild-type mice immunized with mBSA, stimulated them *ex vivo* for 30 min with 20ng/ml IL-6 and monitored changes in pY-STAT1 and pY-STAT3 by intracellular flow cytometry. When compared to wild-type CD4$^+$ T cells from the inguinal lymph node of non-challenged mice, CD4$^+$ T cells from mBSA-immunized mice showed impaired pY-STAT1 detection in response to IL-6 (Fig. 1c). This reduction in pY-STAT1 was particularly evident in activated or memory CD4$^+$ T cells (Fig. 1c).

STAT1 is an important determinant of T cell effector function[20, 21, 22]. We therefore used quantitative PCR to evaluate the effector characteristics of CD4$^+$ T cells from wild-type mice with AIA. Analysis was performed on CD4$^+$ T_N cells and CD4$^+$CD25$^-$CD44^{hi}CD62L^{lo}CD127$^{int\text{-}hi}$ effector memory T cells (T_{EM} cells) from the inguinal lymph nodes of wild-type mice with AIA. *Ahr*, *Il21*, *Rorgt*, *Il17a*, *Ifng* and *Stat3* were all highly expressed in CD4$^+$ T_{EM} cells compared to CD4$^+$ T_N cells (Fig. 1d). In contrast, the expression of *Socs3*, a negative regulator of Jak-STAT signaling, remained comparable in both CD4$^+$ T cell populations (Fig. 1d). In addition, intracellular cytokine staining of CD4$^+$ T_N and CD4$^+$ T_{EM} cells showed that CD4$^+$ T_{EM} cells generated increased amounts of IL-21 (Fig. 1e and Supplementary Fig. 1a). Thus, CD4$^+$ T_N and CD4$^+$ T_{EM} cells showed differences in IL-6 responsiveness.

Control of STAT1 activity is not determined by IL-6R signaling in CD4$^+$ T cells

To determine if T cell subsets display different IL-6 signaling properties, splenic CD4$^+$ T_N cells, CD4$^+$CD25$^-$CD44^{hi}CD62L^{hi}CD127^{hi} central memory T cells (T_{CM} cells), CD4$^+$CD25$^-$CD44^{lo}CD62L^{lo}CD127$^{lo\text{-}int}$ effector T cells (T_{Eff} cells) and CD4$^+$ T_{EM} cells were purified from wild-type mice. These populations showed differences in IL-6R and gp130 expression, but displayed a similar transient activation of pY-STAT3 in response to IL-6 (Fig. 2a and Supplementary Fig. 1b). A strong induction of pY-STAT1 was

observed in IL-6-treated CD4$^+$ T_N cells, while CD4$^+$ T_{CM}, T_{Eff} and T_{EM} cells showed impaired pY-STAT1 activation (Fig. 2a). A similar regulation of pY-STAT1 was also observed in human CD4$^+$ T cells (Supplementary Fig. 1c).

Given that activation-induced shedding of IL-6R may affect IL-6 receptor signaling, we investigated the IL-6 control of pY-STAT1 and pY-STAT3 in splenic CD4$^+$ T_N, T_{CM}, T_{Eff} and T_{EM} cells from wild-type and *Il6ra*$^{-/-}$ mice. IL-6 signaling in *Il6ra*$^{-/-}$ CD4$^+$ T cells was triggered by IL-6 trans-signaling using an IL-6-sIL-6R chimeric fusion protein (HDS)[7, 8]. *Il6ra*$^{-/-}$ CD4$^+$ T cells were not activated by IL-6 alone, but responded to an equimolar concentration of HDS, and all *Il6ra*$^{-/-}$ CD4$^+$ T cells showed increased pY-STAT3 following HDS stimulation (Fig. 2b). While HDS induced pY-STAT1 in *Il6ra*$^{-/-}$ CD4$^+$ T_N cells, changes in pY-STAT1 was not seen in HDS-treated CD4$^+$ T_{CM}, T_{Eff} and T_{EM} cells from *Il6ra*$^{-/-}$ mice (Fig. 2b). Thus, the loss of STAT1 signaling in activated CD4$^+$ T cells is independent of changes in IL-6R regulation. A similar pattern of pY-STAT1 regulation was noted in wild-type CD4$^+$ T cells stimulated with IL-27 or IFN-γ (Fig. 2c and Supplementary Fig. 2d), suggesting the control of STAT1 phosphorylation was not unique to IL-6.

TCR activation regulates IL-6R signaling in CD4$^+$ T cells

To investigate whether prior TCR engagement contributed to the changes in STAT1 activation in activated or memory CD4$^+$ T cells we compared IL-6 signaling in CD4$^+$ T_N cells and CD4$^+$ T cells previously activated with antibodies against CD3 and CD28. Wild-type CD4$^+$ T_N cells were cultured for 72h with antibodies against CD3 and CD28 followed by a 48h culture in fresh media, in the absence of exogenous stimulation. This rest period restored the surface expression of IL-6R on these TCR-experienced effector-like CD4$^+$ T cells (T_{EXP} cells; Supplementary Fig. 2a). While IL-6 stimulation of CD4$^+$ T_{EXP} cells induced pY-STAT3, the activation of pY-STAT1 was minimal when compared to the IL-6-dependent induction of pY-STAT1 in CD4$^+$ T_N cells (Supplementary Fig. 2b,c), indicating CD4$^+$ T cell activation altered the subsequent activation of STAT1 by IL-6.

To test if TCR signaling altered the IL-6-induced activation of STAT1, we generated CD4$^+$ T_{EXP} cells from wild-type CD4$^+$ T_N cells using varying concentrations of co-stimulatory CD3 (0.1-10 μg/ml) and CD28 (0.5-15 μg/ml) antibodies (Supplementary Fig. 3a) and stimulated the expanded CD4$^+$ T_{EXP} cells with IL-6. The IL-6-dependent induction of pY-STAT3 was not affected by differences in antibody concentration. However the suppression of pY-STAT1 in response to IL-6 was sensitive to anti-CD3 antibody treatment with increasing doses of antibody leading to a repression of pY-STAT1 (Supplementary Fig. 3a). Thus, TCR signaling affected the inhibition of pY-STAT1 by IL-6.

We next determined whether changes in STAT1 activation altered the transcriptional output of IL-6. CD4$^+$ T_N, T_{EXP} and T_{EM} cells were stimulated for 6 h with IL-6 followed by transcriptomic analysis. This time point was selected based on the temporal profile of pY-STAT1 and pY-STAT3 detection (Fig. 2a), and the

optimal expression of STAT-target genes (*Ahr*, *Bcl3*, *Bcl6*, *Kat2b*, *Il10*, *Il21*, *Pim1, Stat3*), as determined by Q-PCR (Supplementary Fig. 3b). $CD4^+$ T_N, T_{EXP}, and T_{EM} cells expressed a series of genes that were both common (e.g., *Socs1*, *Sbno2*, *Bcl6*) and unique (e.g., $CD4^+$ T_N – *Cxcr1*, *Tnfrsf14*; $CD4^+$ T_{EXP} – *Gzma*, *Ajuba*; $CD4^+$ T_{EM} – *Ahr*, *Il10, Il21*) to all three $CD4^+$ T cell populations (Fig. 2d and Supplementary Fig. 3c). The number of transcripts enhanced by IL-6 in $CD4^+$ T_{EXP} cells (236) was markedly reduced when compared to the IL-6-dependent induction of transcripts in $CD4^+$ T_N cells (509) (Fig. 2e). The inclusion of anti-CD3+CD28 co-stimulatory antibodies further suppressed the number of genes induced by IL-6 in $CD4^+$ T_{EXP} cells (26), indicating the capacity of TCR activation to replace the signal delivered by IL-6 (Fig. 2e and Supplementary Fig. 3d). Thus, IL-6 controls very distinct patterns of gene regulation in $CD4^+$ T_N, T_{EXP} and T_{EM} cells that may shape the functional properties of these $CD4^+$ T cells.

STAT1 phosphorylation is regulated by PTPN2

We next determined whether TCR activation altered the expression of genes linked with IL-6 receptor signaling in $CD4^+$ T_N, T_{EXP} and T_{EM} cells. No significant differences in the expression of IL-6 receptor subunits (*Il6ra*, *Il6st*), Janus kinases (*Jak1*, *Jak2*, *Tyk2*), STATs (*Stat1*, *Stat3*, *Stat5a*, *Stat5b*) and regulators of IL-6 or Jak-STAT signaling (*Socs1*, *Socs3*, *Pias1*, *Dusp2*, *Cish*, *Arid5a*, *Arid5b*) were observed between these $CD4^+$ T cells (Supplementary Fig. 4a). Thus, the immediate regulation of STAT1 activity in $CD4^+$ T_{EXP} cells and $CD4^+$ T_{EM} cells was not attributed to changes in the make-up of the IL-6 signaling cascade.

To examine how $CD4^+$ T cell activation affected STAT1 signaling we assessed IL-6 responses in wild-type $CD4^+$ T_N and T_{EM} cells using antibodies for serine phosphorylated STAT1 and STAT3 (hereafter pS-STAT1 and pS-STAT3). Intracellular flow cytometry showed that the IL-6 activation of pS-STAT1 and pS-STAT3 was comparable in both $CD4^+$ T cells (Fig. 3a). However, $CD4^+$ T_{EM} cells showed suppressed pY-STAT1 in response to IL-6 (Fig. 3a and Supplementary Fig. 1c). We therefore addressed whether protein phosphatases controlled the tyrosine phosphorylation of STAT1. Treatment of $CD4^+$ T_N and T_{EM} cells with the protein tyrosine phosphatase inhibitor sodium orthovanadate reversed the loss of pY-STAT1 activation in IL-6-stimulated $CD4^+$ T_{EM} cells (Fig. 3a). IL-6 control of pY-STAT3 was unaltered by sodium orthovanadate (Fig. 3a). Analysis of *Ahr, Il21, Socs3* and *Stat3* expression in IL-6-treated $CD4^+$ T_{EM} cells showed that the inclusion of sodium orthovanadate reduced expression of *Il21* and *Socs3* (Fig. 3b). Thus, protein tyrosine phosphatase activity appears integral to the IL-6 control of STAT1 in $CD4^+$ T_{EM} cells.

To identify protein tyrosine phosphatases responsible for the regulation of STAT1 in $CD4^+$ T_{EXP} and T_{EM} cells we compared transcriptomic data from $CD4^+$ T_N, T_{EXP} and T_{EM} cells activated with anti-CD3+CD28 co-stimulatory antibodies. Several protein phosphatases were more highly expressed in $CD4^+$ T_{EXP} and T_{EM} cells than $CD4^+$ T_N cells, and included the protein tyrosine phosphatases *Ptpn2* and *Ptpn22* (Fig. 3c).

Flow cytometry showed that PTPN2 was more highly expressed in $CD4^+$ T_{EM} cells than $CD4^+$ T_N cells (Fig. 4a). *Il6ra*$^{-/-}$ $CD4^+$ T_{EM} cells had comparable expression of PTPN2 to wild-type $CD4^+$ T_{EM} cells (Fig. 4b), indicating that PTPN2 expression was independent of IL-6 signaling. To confirm the relevance of these findings to pathology we conducted immunohistochemistry of joint tissue from wild-type mice with AIA. Synovial $CD3^+$ T cells showed enhanced expression of PTPN2 and low pY-STAT1 staining (Fig. 4c). Similarly, flow cytometry of IL-6-stimulated $CD4^+$ T_{EM} cells revealed that PTPN2 expression correlated with suppression of pY-STAT1 (Fig. 4b, Supplementary Fig. 4b). We next investigated IL-6 signaling in $CD4^+$ T_N and T_{EXP} cells from whole genome C57Bl/6 *Ptpn22*$^{-/-}$ mice and *Lck*-Cre *Ptpn2*$^{fl/fl}$ mice, which lack PTPN2 in $CD4^+$ T cells. As controls we used IL-6-treated $CD4^+$ T_N and T_{EXP} cells isolated from C57Bl/6 wild-type mice (for PTPN22) or C57Bl/6 *Ptpn2*$^{fl/fl}$ littermates. IL-6 activated pY-STAT1 in both *Lck*-Cre *Ptpn2*$^{fl/fl}$ and *Ptpn22*$^{-/-}$ $CD4^+$ T_{EXP} cells (Fig. 4d). When compared to IL-6 stimulated $CD4^+$ T_{EXP} cells from *Lck*-Cre *Ptpn2*$^{fl/fl}$ mice, the recovery of pY-STAT1 activity in IL-6 treated *Ptpn22*$^{-/-}$ $CD4^+$ T_{EXP} cells was less obvious (Fig. 4d). This possibly reflected a lower expression of *Ptpn22* in $CD4^+$ T_{EXP} cells (Fig. 3c). Thus, PTPN2 acted as a repressor of IL-6-induced STAT1 tyrosine phosphorylation in activated $CD4^+$ T cells.

We next explored whether PTP activity affected the production of IL-17A and IL-21 in $CD4^+$ T_{EM} cells. Intracellular flow cytometry indicated that *Lck*-Cre *Ptpn2*$^{fl/fl}$ and *Ptpn22*$^{-/-}$ $CD4^+$ T_{EM} cells mice generated less IL-17A and IL-21 than $CD4^+$ T_{EM} cells from *Ptpn2*$^{fl/fl}$ littermates or wild-type mice (Fig**.** 4e, Supplementary Fig. 4c). Moreover, ImageStream analysis showed the co-localization of PTPN2 with non-phosphorylated STAT1 in wild-type $CD4^+$ T_{EM} cells (Fig. 4f). Thus, PTPN2, and to a lesser extent PTPN22, regulated STAT1 signaling in activated and memory $CD4^+$ T cells.

T cell activation re-tunes the transcriptional output of IL-6 in $CD4^+$ T_{EM} cells

Next, we compared the transcriptional output of IL-6 in $CD4^+$ T_N, T_{EXP} and T_{EM} cells. Analysis was confined to significantly regulated genes (p<0.05) that displayed both a relative signal intensity of >150 and >1.5 fold alteration in expression. Circos visualization identified a number of genes that were under IL-6 control in $CD4^+$ T_N (225), T_{EXP} (31) and T_{EM} (180) cells (Fig. 5a). Hierarchical clustering and validation of selected gene targets identified IL-6 gene signatures that were either common to all three $CD4^+$ T cells or uniquely expressed by a particular population (Supplementary Fig. 3c). Genes regulated by IL-6 in $CD4^+$ T_N, T_{EXP} and T_{EM} cells were mainly STAT3 target genes[23, 24] and included genes that encoded transcriptional regulators (e.g., *Bcl3*, *Bcl6*, *Etv6*), co-repressors (e.g., *Sbno2*, *Muc1*) and negative regulators (e.g., *Socs3*, *Pim1*, *Batf*) of transcription factors such as STAT3, NF-κB and AP1 (Supplementary Fig. 3c).

Next, we conducted a molecular pathway analysis of the transcriptomic data from IL-6-treated $CD4^+$ T_N, T_{EXP} and T_{EM} cells (Fig. 5b). We also mapped these datasets against publicly-available transcriptomic data

from IL-6-stimulated *Stat1*$^{-/-}$ and *Stat3*$^{-/-}$ CD4$^+$ T cells (Fig. 5c)[20]. This analysis identified a series of STAT1-regulated genes commonly associated with interferon (e.g., *Irf8*, *Gbp2*, *Gbp5, Gbp6, Stat1, Parp9*). In contrast, STAT3-regulated genes displayed greater functional diversity and were implicated in interleukin signaling, immune activation, proliferation, catabolism and metabolism (e.g., *Socs3*, *Bcl3*, *Il6r, Kat2b*) (Fig. 5b,c). This collective approach demonstrated that STAT1 and STAT3 regulated very distinct patterns of gene expression in IL-6 stimulated CD4$^+$ T_N, T_{EXP} and T_{EM} cells (Fig. 5b,c). For example, when compared with IL-6 stimulated CD4$^+$ T_N cells, activation with IL-6 enhanced the expression of genes associated with prolonged lymphocyte survival and memory (e.g., *Hmox1*, *Myc*, *Cd83*), and regulatory (e.g., *Lag3, Il10, Foxp3*) or effector (e.g., *Ahr, Il21, Ifng*) characteristics in CD4$^+$ T_{EM} cells.

We next performed ChIP-seq in IL-6-stimulated CD4$^+$ T_N and T_{EM} cells. Sequencing peaks displaying a 4-fold increase above input (P<0.0001; FDR 0.05) were aligned to the genome and assigned to transcription start sites (TSS), exons and introns (Fig. 6 and Supplementary Fig. 5). Peaks located in undefined intergenic regions were excluded from the analysis. ChIP-seq of IL-6-stimulated CD4$^+$ T_N cells identified 1625 peaks associated with STAT1 and 602 peaks for STAT3 (Fig. 6a). The number of STAT1 (446) and STAT3 (552) peaks was reduced in CD4$^+$ T_{EM} cells (Fig. 6a). To understand the regulatory properties of STAT1 and STAT3 we first confined our analysis to peaks residing within TSS regions (Fig. 6b and Supplementary Fig. 5). Sequencing peaks that mapped to defined gene promoters were correlated against corresponding transcriptomic data from IL-6-treated CD4$^+$ T_N and T_{EM} cells (Fig. 6c and Supplementary Fig. 5). STAT1 and STAT3 showed substantially reduced binding to TSS regions in CD4$^+$ T_{EM} cells compared to CD4$^+$ T_N cells (Fig. 6b,c,d). Very few genes shared STAT1 and STAT3 binding (e.g., *Stat3*, *Stat5b*, *Icam1*, *Socs3*, *Sigirr*, and *Akt2*) (Fig. 6b,d), and these co-regulated genes were largely restricted to CD4$^+$ T_N cells (Fig 6b,d). *Stat3* was the only gene that was bound by both STAT1 and STAT3 in CD4$^+$ T_{EM} cells (Fig. 6c). To determine the specificity of these DNA-transcription factor interactions we used computational tools to identify consensus DNA motifs for STAT1 and STAT3 binding (Supplementary Fig. 5c). Analysis of ChIP-seq datasets from IL-6-treated CD4$^+$ T_N and T_{EM} cells identified sequences resembling an IFN-regulated STAT responsive element (ISRE; E-value 5.9e-040) for STAT1 binding, and sequences homologous to a gamma-activated sequence (GAS; E-value 1.2e-115) for STAT3 (Supplementary Fig. 5c). We also identified consensus motifs for other transcription factors including SP1 and C2H2 Zn-finger transcription factor proteins (Supplementary Fig. 5c) and ChIP-qPCR showed STAT1 and STAT3 bound to SP1 consensus binding sequences (Supplementary Fig. 5d and Supplementary Table 2). Thus, transcriptional differences between IL-6 stimulated CD4$^+$ T_N and T_{EM} cells are shaped by STAT1 and STAT3 docking to both classical STAT-responsive elements and DNA motifs that suggested a regulatory interplay with other transcription factors in CD4$^+$ T_N and T_{EM} cells.

Genes under IL-6 control in CD4$^+$ T_{EM} cells are regulated at distal promoter regions

Next we investigated the canonical pathways associated with the genes that were bound with STAT1 or STAT3 in IL-6-treated $CD4^+$ T_N and T_{EM} cells. Bioinformatic analysis identified a selective enrichment of genes involved in disease processes, catabolism and cytokine signaling in $CD4^+$ T_{EM} cells as compared to $CD4^+$ T_N cells (Supplementary Fig. 6a and Supplementary Table 3). Many of the genes associated with these pathways were distinct from those showing STAT1 or STAT3 binding to TSS (Fig. 6b), suggesting that genes under IL-6 regulation in $CD4^+$ T_{EM} cells may be controlled by STAT1 and STAT3 binding to distal promoter regions. To identify possible mechanisms that may explain this distal regulation we evaluated whether STAT1 and STAT3 peaks aligned with enhancer regions displaying enriched binding of the histone acetyl-transferase P300 (hereafter P300 enhancer elements[25, 26, 27, 28]). STAT1 and STAT3 ChIP-seq datasets from IL-6-treated $CD4^+$ T_N or T_{EM} cells were mapped against publicly-available P300 ChIP-seq data from mouse $CD4^+$ T cells polarized *in vitro* into T_H1, T_H2 or T_H17 cells[28] (Supplementary Fig. 6b and Supplementary Table 4). A combined analysis of IL-6-treated $CD4^+$ T_N and T_{EM} cells identified 558 genes that bound P300 in association with either STAT1 or STAT3 (Fig. 7a,b). In IL-6-stimulated $CD4^+$ T_N and T_{EM} cells we identified 215 genes that displayed alternate binding of STAT1 or STAT3 in $CD4^+$ T_N and T_{EM} cells (Fig. 7b). These genes were selectively induced or repressed by IL-6 in $CD4^+$ T_{EM} cells (Fig. 7b, Supplementary Table 5). Among these, 208 genes aligned with genes bound by P300 in T_H17 cells[28]. These included genes linked with proliferation and survival (e.g., *Vmp1*, *Rbpj*, *Fasl*), immune regulation (e.g., *Cd200*, *Cish*, *Ctla4*, *Cd69*), alternate lineage fates (e.g., *Ahr*, *Batf*, *Bcl6*, *Cxcr5*, *Etv6*, *Fosl2, Irf4*, *Stat3*) or differences in T cell effector function (e.g., *Il10*, *Il21*, *Il4ra*, *Il17a*, *Il17ra*, *Il21r*) (Supplementary Table 5). This analysis indicated that genes controlled by IL-6 in $CD4^+$ T_N and T_{EM} cells are associated with P300 enhancer elements that are potentially activated or suppressed by changes in the pattern of STAT1 or STAT3 binding.

Among the 215 genes regulated by IL-6 in $CD4^+$ T_{EM} cells, 80 displayed STAT1 or STAT3 binding in ChIP-seq data from IL-6 activated $CD4^+$ T_N cells, but not in IL-6 treated $CD4^+$ T_{EM} cells (Fig. 7c). This suggested that the binding of these transcription factors to these sites acted as repressors of gene activation. ChIP-seq analysis of the other 135 genes showed that some form of STAT1 or STAT3 binding to P300 enhancer elements was retained in both IL-6 stimulated $CD4^+$ T_N and T_{EM} cells (Fig. 7c and Supplementary Fig. 6b). These included *Il10*, *Il21*, *Il21r*, *Bcl3*, *Batf*, *Junb*, *Socs1* and *Cd274* (Fig.7c). Circos visualization illustrated how the binding of STAT1 and STAT3 to these promoters differed between IL-6 stimulated $CD4^+$ T_N and T_{EM} cells (Fig. 7c). We identified 5 discrete patterns of STAT1 and STAT3 binding – pattern 1 ($CD4^+$ T_N cells: no STAT binding; T_{EM} cells: STAT1), pattern 2 ($CD4^+$ T_N cells: STAT1, STAT3; T_{EM} cells: STAT3), pattern 3 ($CD4^+$ T_N cells: STAT3; T_{EM} cells: STAT3), pattern 4 ($CD4^+$ T_N cells: STAT1; T_{EM} cells: STAT3) and pattern 5 ($CD4^+$ T_N cells: no STAT binding; T_{EM} cells: STAT3) (Fig.7d). Computational analysis of the genes affiliated to each pattern revealed links with the cytokine control of T cell proliferation, differentiation and survival (Fig. 7d, Supplementary Fig. 6b and Supplementary Table 6). This was particularly apparent in pattern 2,

and to a lesser extent, pattern 3 and 5. Promoter regions assigned to pattern 2 displayed binding of STAT1 and STAT3 in IL-6 stimulated $CD4^+ T_N$ cells, but showed a loss of STAT1 in IL-6 activated $CD4^+ T_{EM}$ cells. Genes identified with this form of STAT regulation included *Junb*, *Il4ra*, *Cd274* and *Socs1* (Fig.7c and Supplementary Fig.6b) and suggested a potential link to the PTPN2-regulated of pY-STAT1. We therefore conducted a ChIP-qPCR analysis of STAT1 binding to the promoters of *Junb*, *Il4ra*, *Cd274* and *Socs1* in IL-6-stimulated Lck-Cre $Ptpn2^{fl/fl}$ and $Ptpn2^{fl/fl}$ $CD4^+ T_{EM}$ cells. STAT1 binding to these promoters was specifically enriched in DNA samples from Lck-Cre $Ptpn2^{fl/fl}CD4^+ T_{EM}$ cells as compared to control $Ptpn2^{fl/fl}$ $CD4^+ T_{EM}$ cells (Fig. 7e). In contrast, the binding of STAT1 to the TSS regions of *Stat3* and *Irf1* remained unaltered, and DNA samples from Lck-Cre $Ptpn2^{fl/fl}CD4^+ T_{EM}$ cells and control $Ptpn2^{fl/fl}$ $CD4^+ T_{EM}$ cells showed similar enrichment for STAT1 (Fig. 7e). Thus, PTPN2 activity determined STAT1 binding to specific gene promoter regions in IL-6 activated $CD4^+ T_{EM}$ cells.

PTPN2 correlates with indices of synovial pathology in rheumatoid arthritis patients

Many of the genes identified in IL-6 stimulated $CD4^+ T_{EM}$ cells contribute to the generation and maintenance of effector T cells associated with autoimmunity (Supplementary Table 6). We therefore investigated the relationship between *PTPN2* and *PTPN22* and these IL-6-regulated genes in RNA-seq datasets from synovial tissues biopsies of 87 patients with rheumatoid arthritis. Expression of *PTPN2* and *PTPN22* in these biopsy samples was compared against corresponding histological staining of the inflamed synovium for the lymphocyte markers CD3 and CD20 by immunohistochemistry. Analysis revealed a close correlation between PTPN2 and CD3 and CD20 (Fig 8a). This association was particularly evident in synovial biopsies displaying evidence of ectopic lymphoid-like structures (lymphoid-rich) and synovitis with a prominent mononuclear cell infiltrate (myeloid-rich) (Fig. 8b)[29]. In contrast, *PTPN22* displayed a more uniform pattern of expression within the inflamed synovium and showed no correlation with lymphocyte markers or the type of synovial pathology (Fig. 8a,b). To establish a possible link between PTPN2 and the synovial expression of genes controlled by IL-6 in activated or memory $CD4^+$ T cells *PTPN2* was compared against the synovial expression of *IL21*, *IL17A*, *CD274* and *SOCS1*. Analysis of synovial RNA-seq datasets showed a correlation between *PTPN2* and *IL21*, *IL17A*, *CD274* and *SOCS1* (Fig. 8c). This relationship was particularly evident in both lymphoid-rich and myeloid-rich synovitis (Fig. 8c). No clear correlation was observed between *PTPN22* and these inflammatory markers (Fig. 8c). Thus, in human synovial pathology, *PTPN2* associates with the involvement of lymphocytes in the disease process and corresponds with the expression of several inflammatory mediators linked to the regulation of STAT1 by PTP enzymes.

Discussion

Through analysis of Jak-STAT signalling in $CD4^+ T_N$ and T_{EM} cells we identified that protein tyrosine phosphatases induced as a response to $CD4^+ T_N$ cell activation altered the transcriptional output of IL-6 in $CD4^+ T_{EM}$ cells. Our investigation showed that inhibition of STAT1 phosphorylation by PTPN2 affected the expression of certain STAT-regulated target genes in activated or memory $CD4^+$ T cells. Thus, protein tyrosine phosphatases have the capacity to modify the way particular T cell subsets sense and interpret common cytokine cues. Whilst the study focussed on the biology of IL-6, this mechanism may also shape the transcriptional output of other lymphokines in $CD4^+$ T cells.

Protein phosphatases including dual specificity protein phosphatases (DUSP) and protein tyrosine phosphatases (PTP) can regulate Jak-STAT signaling[30, 31]. For example, PTPN2 and PTPN11 control the phosphorylation of STAT1 in fibroblasts[32, 33]. We showed that protein tyrosine phosphatases restrained IL-6 signaling through STAT1 in activated and memory $CD4^+$ T cells. Transcriptional profiling of PTP expression in $CD4^+$ T cells identified several candidate enzymes that were induced following $CD4^+ T_N$ activation, including PTPN2, PTPN22 and DUSP2. Because DUSP2 inhibits signaling through STAT3 and restricts T_H17 differentiation[30], we assessed whether PTPN2 and PTPN22 affected STAT1 phosphorylation. PTPN2 and PTPN22 inhibited STAT1 activity, but had a less obvious impact on STAT3 activity. This observation might indicate a physical interaction between these PTP and STAT1.

PTPN2 and PTPN22 control various lymphocyte responses, and individuals with genetic polymorphisms in *PTPN2* or *PTPN22* frequently show increased susceptibility to autoimmune disease[34, 35]. The ability of PTPN2 and PTPN22 to control Jak-STAT signaling may contribute to these outcomes through the control of immune activation, tolerance and autoimmunity. Our data showed that synovial *PTPN2* was highly expressed in lymphoid-rich synovitis. This form of joint pathology is defined by the presence of functional ectopic lymphoid aggregates within the inflamed synovium[36]. Significantly, PTPN2 has been linked with the regulation of follicular T_H cells and the activation of T and B cell responses[37, 38, 39, 40]. Our investigation showed that PTPN2 controlled the expression of genes commonly associated with ectopic lymphoid-like structures. For example, PTPN2-control of STAT1 phosphorylation was shown to affect the transactivation of inflammatory cytokines (e.g., IL-17A, IL-21), transcription factors (e.g., Bcl6), immune checkpoint regulators (e.g., CD274) and homeostatic chemokine receptors (e.g., CXCR4, CXCR5) involved in the activity or spatial organization of lymphoid aggregates[36]. The gene signature identified through our screen may therefore predict the efficacy of adoptive immunotherapy and vaccination strategies, or response to biological drug therapies.

ChIP-seq of STAT1 and STAT3 in IL-6-treated $CD4^+ T_N$ and T_{EM} cells showed that both transcription factors bound to consensus motifs for STAT proteins (e.g., ISRE, GAS), and sequences specific for other

transcription factors (e.g., SP1-like proteins)[41, 42, 43, 44]. While the binding of STATs to these genomic sites requires further analysis, our results suggested that the induction of PTPN2 in activated $CD4^+$ T cells affected the expression of STAT-regulated genes controlled by P300 enhancer elements. Many of the genes associated with these enhancers were induced by IL-6 in $CD4^+$ T_{EM} cells and included genes commonly associated with T_H1, T_H2, T_H17 or T_{FH} cells[27, 28]. These activities fit with the capacity of IL-6 to govern $CD4^+$ T cell memory[4, 5, 45, 46]. For example, IL-6 renders antigen-specific T cells refractory to suppression by regulatory T cells[56, 57]. However, IL-6 signaling is not critical for the generation or maintenance of $CD4^+$ memory cells[4, 6]. Instead, our data revealed that IL-6 promotes the effector or functional characteristics of $CD4^+$ T_{EM} cells. This contrasts with the activities of IL-23, which regulates memory recall through the control of cell-cycle progression and proliferation[7, 47, 48]. Thus, PTPN2 control of STAT1 may support $CD4^+$ T cell memory responses by shaping effector memory functions or prolonging lymphocyte survival. Such findings may be relevant to our understanding of how T cells become released from anergy and might explain how T cells become directed down a commitment pathway as a response to specific TCR antigens[39, 49, 50].

Acknowledgements

This manuscript is dedicated in fond memory of J. Uceda Fernandez, a dearly loved friend and colleague who was tragically taken from us on the 29th August 2018. Remembered forever.

Versus Arthritis (Reference 20770, 19796 awarded to SAJ, NMW & GWJ), Hoffmann la Roche (to SAJ), Kidney Research UK (to SAJ) and the National Health and Medical Research Council of Australia (to TT) provided grant support for this project. GWJ is recipient of a Versus Arthritis Career Development Fellowship (Reference 20305). JUF held a la Caixa PhD Studentship administered through the British Council, and BCC is supported by a PhD studentship from the Systems Immunity University Research Institute at Cardiff. JL is recipient of a Rutherford Fellowship Grant. Analysis of synovial tissues was conducted with support from the Medical Research Council (to CJP; Reference 36661) and the Versus Arthritis funded Experimental Arthritis Treatment Centre (to CJP; Reference 20022). PRT is recipient of a Wellcome Trust Investigator Award (107964/Z/15/Z) and receives funding through the UK Dementia Research Institute. Bioinformatic analysis was developed with support from the Systems Immunity University Research Institute in Cardiff. The authors would like to thank Yuka Kanno, Chris Hunter, Stephen Turner, Toshi Nakayama, Magdalena Czubala, Rachel Errington, Atsushi Onodera, Kiyoshi Hirahara and John O'Shea for their advice, constructive opinions and kind support.

Author contributions

SAJ, GWJ, ACF and JPT wrote the text and prepared the figures for the paper. All authors reviewed and approved the final manuscript draft. SAJ, GWJ, TT, NMW, CP, PRT, CJP, JPT, ACF designed the study. BCC, RA, ML, MJT, BS, ACF, JPT and NMW conducted bioinformatic, biostatistical, and molecular pathway analyses. Laboratory based studies were performed by JPT, ACF, FW, MJT, XL, JUF, ADS, JL, DH and DM.

Competing interests

SAJ has received funding support from Hoffman-La Roche, GlaxoSmithKline, Ferring Pharmaceuticals and NovImmune SA, and during the last 5 years he has acted as an advisory consultant for Roche, Chugai Pharmaceuticals, NovImmune SA, Genentech, Sanofi Regeneron, Johnson & Johnson, Janssen Pharmaceuticals, Eleven Biotherapeutics.

References

1. MacLeod, M.K., Kappler, J.W. & Marrack, P. Memory CD4 T cells: generation, reactivation and re-assignment. *Immunology* **130**, 10-15 (2010).

2. O'Shea, J.J. *et al.* The JAK-STAT pathway: impact on human disease and therapeutic intervention. *Annu Rev Med* **66**, 311-328 (2015).

3. Hunter, C.A. & Jones, S.A. IL-6 as a keystone cytokine in health and disease. *Nat Immunol* **16**, 448-457 (2015).

4. Nish, S.A. *et al.* T cell-intrinsic role of IL-6 signaling in primary and memory responses. *Elife* **3**, e01949 (2014).

5. Longhi, M.P. *et al.* Interleukin-6 is crucial for recall of influenza-specific memory CD4 T cells. *PLoS Pathog* **4**, e1000006 (2008).

6. Strutt, T.M. *et al.* Direct IL-6 Signals Maximize Protective Secondary CD4 T Cell Responses against Influenza. *The Journal of Immunology* (2016).

7. Jones, G.W. *et al.* Loss of CD4+ T cell IL-6R expression during inflammation underlines a role for IL-6 trans signaling in the local maintenance of Th17 cells. *J Immunol* **184**, 2130-2139 (2010).

8. Fielding, C.A. *et al.* Interleukin-6 signaling drives fibrosis in unresolved inflammation. *Immunity* **40**, 40-50 (2014).

9. Harker, J.A., Lewis, G.M., Mack, L. & Zuniga, E.I. Late interleukin-6 escalates T follicular helper cell responses and controls a chronic viral infection. *Science* **334**, 825-829 (2011).

10. Briso, E.M., Dienz, O. & Rincon, M. Cutting edge: soluble IL-6R is produced by IL-6R ectodomain shedding in activated CD4 T cells. *J Immunol* **180**, 7102-7106 (2008).

11. Teague, T.K. *et al.* Activation-induced inhibition of interleukin 6-mediated T cell survival and signal transducer and activator of transcription 1 signaling. *J Exp Med* **191**, 915-926 (2000).

12. Hong, C. *et al.* Interleukin-6 expands homeostatic space for peripheral T cells. *Cytokine* **64**, 532-540 (2013).

13. Chtanova, T. *et al.* Identification of T cell-restricted genes, and signatures for different T cell responses, using a comprehensive collection of microarray datasets. *J Immunol* **175**, 7837-7847 (2005).

14. Curnow, S.J. *et al.* Inhibition of T cell apoptosis in the aqueous humor of patients with uveitis by IL-6/soluble IL-6 receptor trans-signaling. *J Immunol* **173**, 5290-5297 (2004).

15. Nowell, M.A. *et al.* Therapeutic targeting of IL-6 trans signaling counteracts STAT3 control of experimental inflammatory arthritis. *J Immunol* **182**, 613-622 (2009).

16. Atreya, R. *et al.* Blockade of interleukin 6 trans signaling suppresses T-cell resistance against apoptosis in chronic intestinal inflammation: evidence in crohn disease and experimental colitis in vivo. *Nat Med* **6**, 583-588 (2000).

17. Liao, W., Lin, J.X., Wang, L., Li, P. & Leonard, W.J. Modulation of cytokine receptors by IL-2 broadly regulates differentiation into helper T cell lineages. *Nat Immunol* **12**, 551-559 (2011).

18. Villarino, A.V., Kanno, Y. & O'Shea, J.J. Mechanisms and consequences of Jak-STAT signaling in the immune system. *Nat Immunol* **18**, 374-384 (2017).

19. Costa-Pereira, A.P. *et al.* Mutational switch of an IL-6 response to an interferon-gamma-like response. *Proc Natl Acad Sci U S A* **99**, 8043-8047 (2002).

20. Hirahara, K. *et al.* Asymmetric Action of STAT Transcription Factors Drives Transcriptional Outputs and Cytokine Specificity. *Immunity* **42**, 877-889 (2015).

21. Peters, A. *et al.* IL-27 Induces Th17 Differentiation in the Absence of STAT1 Signaling. *J Immunol* **195**, 4144-4153 (2015).

22. Jones, G.W. *et al.* Exacerbated inflammatory arthritis in response to hyperactive gp130 signalling is independent of IL-17A. *Ann Rheum Dis* **72**, 1738-1742 (2013).

23. Anderson, A.E. *et al.* IL-6-driven STAT signalling in circulating CD4+ lymphocytes is a marker for early anticitrullinated peptide antibody-negative rheumatoid arthritis. *Ann Rheum Dis* **75**, 466-473 (2016).

24. Pratt, A.G. *et al.* A CD4 T cell gene signature for early rheumatoid arthritis implicates interleukin 6-mediated STAT3 signalling, particularly in anti-citrullinated peptide antibody-negative disease. *Ann Rheum Dis* **71**, 1374-1381 (2012).

25. Hnisz, D. *et al.* Super-enhancers in the control of cell identity and disease. *Cell* **155**, 934-947 (2013).

26. Whyte, W.A. *et al.* Master transcription factors and mediator establish super-enhancers at key cell identity genes. *Cell* **153**, 307-319 (2013).

27. Vahedi, G. *et al.* Super-enhancers delineate disease-associated regulatory nodes in T cells. *Nature* **520**, 558-562 (2015).

28. Ciofani, M. *et al.* A validated regulatory network for Th17 cell specification. *Cell* **151**, 289-303 (2012).

29. Humby, F. *et al.* Evaluation of Minimally Invasive, Ultrasound-guided Synovial Biopsy Techniques by the OMERACT Filter--Determining Validation Requirements. *J Rheumatol* **43**, 208-213 (2016).

30. Lu, D. *et al.* The phosphatase DUSP2 controls the activity of the transcription activator STAT3 and regulates T17 differentiation. *Nat Immunol* (2015).

31. Bohmer, F.D. & Friedrich, K. Protein tyrosine phosphatases as wardens of STAT signaling. *JAKSTAT* **3**, e28087 (2014).

32. ten Hoeve, J. *et al.* Identification of a nuclear Stat1 protein tyrosine phosphatase. *Mol Cell Biol* **22**, 5662-5668 (2002).

33. Wu, T.R. *et al.* SHP-2 is a dual-specificity phosphatase involved in Stat1 dephosphorylation at both tyrosine and serine residues in nuclei. *J Biol Chem* **277**, 47572-47580 (2002).

34. Hinks, A. *et al.* Association between the PTPN22 gene and rheumatoid arthritis and juvenile idiopathic arthritis in a UK population: further support that PTPN22 is an autoimmunity gene. *Arthritis Rheum* **52**, 1694-1699 (2005).

35. Sharp, R.C., Abdulrahim, M., Naser, E.S. & Naser, S.A. Genetic Variations of PTPN2 and PTPN22: Role in the Pathogenesis of Type 1 Diabetes and Crohn's Disease. *Front Cell Infect Microbiol* **5**, 95 (2015).

36. Pitzalis, C., Jones, G.W., Bombardieri, M. & Jones, S.A. Ectopic lymphoid-like structures in infection, cancer and autoimmunity. *Nat Rev Immunol* **14**, 447-462 (2014).

37. Wiede, F., Sacirbegovic, F., Leong, Y.A., Yu, D. & Tiganis, T. PTPN2-deficiency exacerbates T follicular helper cell and B cell responses and promotes the development of autoimmunity. *J Autoimmun* **76**, 85-100 (2017).

38. Wiede, F. *et al.* T cell protein tyrosine phosphatase attenuates T cell signaling to maintain tolerance in mice. *J Clin Invest* **121**, 4758-4774 (2011).

39. Salmond, R.J., Brownlie, R.J., Morrison, V.L. & Zamoyska, R. The tyrosine phosphatase PTPN22 discriminates weak self peptides from strong agonist TCR signals. *Nat Immunol* **15**, 875-883 (2014).

40. Wiede, F., La Gruta, N.L. & Tiganis, T. PTPN2 attenuates T-cell lymphopenia-induced proliferation. *Nat Commun* **5**, 3073 (2014).

41. Look, D.C., Pelletier, M.R., Tidwell, R.M., Roswit, W.T. & Holtzman, M.J. Stat1 depends on transcriptional synergy with Sp1. *J Biol Chem* **270**, 30264-30267 (1995).

42. Cantwell, C.A., Sterneck, E. & Johnson, P.F. Interleukin-6-specific activation of the C/EBPdelta gene in hepatocytes is mediated by Stat3 and Sp1. *Mol Cell Biol* **18**, 2108-2117 (1998).

43. Zhang, Z., Jones, S., Hagood, J.S., Fuentes, N.L. & Fuller, G.M. STAT3 acts as a co-activator of glucocorticoid receptor signaling. *J Biol Chem* **272**, 30607-30610 (1997).

44. Zhu, M., John, S., Berg, M. & Leonard, W.J. Functional association of Nmi with Stat5 and Stat1 in IL-2- and IFNgamma-mediated signaling. *Cell* **96**, 121-130 (1999).

45. Kasahara, Y. *et al.* Role of interleukin 6 for differential responsiveness of naive and memory CD4+ T cells in CD2-mediated activation. *J Exp Med* **172**, 1419-1424 (1990).

46. Beagley, K.W. *et al.* Peyer's patch B cells with memory cell characteristics undergo terminal differentiation within 24 hours in response to interleukin-6. *Cytokine* **3**, 107-116 (1991).

47. Lee, Y.K. *et al.* Late developmental plasticity in the T helper 17 lineage. *Immunity* **30**, 92-107 (2009).

48. Haines, C.J. *et al.* Autoimmune memory T helper 17 cell function and expansion are dependent on interleukin-23. *Cell Rep* **3**, 1378-1388 (2013).

49. Mohrs, M., Lacy, D.A. & Locksley, R.M. Stat signals release activated naive Th cells from an anergic checkpoint. *J Immunol* **170**, 1870-1876 (2003).

537 50. van Panhuys, N., Klauschen, F. & Germain, R.N. T-cell-receptor-dependent signal intensity
538 dominantly controls CD4(+) T cell polarization In Vivo. *Immunity* **41**, 63-74 (2014).
539

Figure Legends-

Figure 1. Infiltrating T-cells showed impaired STAT1 activity in response to arthritis induction. (a) Representative H&E staining of knee joints at day 10 post disease induction (antigen-induced arthritis, AIA) (bar: 500µm); boxed area shows the location of the immunofluorescence. Representative immunofluorescence with antibodies against CD3 (red), pY-STAT1 or pY-STAT3 (green) is shown together with DAPI counterstaining (blue) (bar: 100µm). Graph shows the proportion of $CD3^+$ T cells displaying either pY-STAT1 or pY-STAT3 (n=3). **(b)** Phosphorylation of STAT1 and STAT3 by flow cytometry of infiltrating synovial $CD4^+$ T cells during AIA after stimulation with 20ng/ml IL-6 compare to $CD4^+$ T_N cells. **(c)** Representative flow cytometry of pY-STAT1 and pY-STAT3 in $CD4^+$ T cells extracted from inguinal lymph nodes of mBSA challenged (n=4) and non-challenged mice (control) (n=3) following stimulation with 20ng/ml IL-6 for 30 min. Graphs show quantification of pY-STAT1 and pY-STAT3 activity in $CD4^+$ T_N and $CD4^+$ T_{EM} cells (n=4). **(d)** Quantitative PCR of *Ahr, Ifng, Il17a, Il21, Rorc, Socs3 and Stat3* in $CD4^+$ T_N (n=4) and $CD4^+$ T_{EM} cells (n=2) extracted from inguinal lymph nodes of mBSA challenged mice. **(e)** Intracellular flow cytometry analysis of IL-21 production in $CD4^+$ T_N and $CD4^+$ T_{EM} cells extracted from inguinal lymph nodes after 4 hours stimulation with PMA, ionomycin and monensin (n=4). Data are representative of three independent experiments (c,e), two independent experiments (a,b) and one experiment involving biological replicates (d). ****P<0.0001, **P<0.01, *P<0.05 (Two-tailed unpaired Student's t test (a,b,d,e) and one-way ANOVA test with Tukey's multiple comparison test (c). Data are shown as mean ± s.d.)

Figure 2. $CD4^+$ T cell subsets show different response to IL-6. (a) Representative flow cytometry analysis of STAT1 and STAT3 responses in naïve (T_N), central memory (T_{CM}), effector (T_{Eff}) and effector memory (T_{EM}) $CD4^+$ T cells after 30 min IL-6 stimulation (20ng/ml). Numbers indicate the percentage of pY-STAT1 or pY-STAT3 staining. Temporal changes in pY-STAT1 and pY-STAT3 are shown for each T cell subset following IL-6 stimulation (n=3). **(b)** Detection of pY-STAT1 and pY-STAT3 in $CD4^+$ T_N, $CD4^+$ T_{CM}, $CD4^+$ T_{Eff} and $CD4^+$ T_{EM} cells from WT and *IL6ra*$^{-/-}$ mice. $CD4^+$ T cells were stimulated for 30 min with an equimolar concentration of IL-6 or an IL-6-sIL-6R fusion protein (HDS) (n=3). **(c)** Intracellular flow cytometry analysis of pY-STAT1 in $CD4^+$ T cells following 30 min stimulation with IL-6, IL-27 or IFNγ (20ng/ml) (n=3). **(d)** Microarray expression data is presented for $CD4^+$ T_N (n=3), $CD4^+$ T_{EM} (n=3), and *in vitro* expanded $CD4^+$ effector-like T cells (See Supplementary Fig.2a, $CD4^+$ T_{EXP}) (n=4) treated with 20ng/ml IL-6 for 6 hours. Analysis was confined to genes displaying both a relative signal intensity of >150 and >1.5-fold alteration in expression following IL-6 treatment (P<0.05). Heat map is hierarchically clustered based in the relative expression (Z-score) (left panel) or Fold change (right panel). **(e)** Volcano plots displaying IL-6 regulated gene expression in $CD4^+$ T_N and $CD4^+$ T_{EXP} cells stimulated with IL-6 (20ng/ml) or in combination with antibodies against CD3 and CD28. An interactive figure can be found on-line (http://jones-

cytokinelab.co.uk/NI2019/figure2d.shtml). Data are representative of two independent experiments (a,c) and one experiment involving biological replicates (b,d,e). ***P<0.001 *P<0.05 (Two-tailed unpaired Student's t test (a) and one-way ANOVA with Tukey's multiple comparison test (b,c). Data are shown as mean ± s.e.m).

Figure 3. Induction of protein tyrosine phosphatases following T-cell activation limits STAT1 signalling. **(a)** $CD4^+$ T_N and $CD4^+$ T_{EM} cells were pre-treated for 5 min with 5mM sodium orthovanadate (vanadate) prior to IL-6 (20ng/ml) stimulation for 30 min. Changes in pY-STAT1 and pY-STAT3 activity were monitored by intracellular flow cytometry (MFI). A comparable analysis of pS-STAT1 and pS-STAT3 is shown as a control (n=3). **(b)** Quantitative PCR for *Ahr*, *Il21*, *Stat3* and *Socs3* after vanadate pre-treatment and 20ng/ml IL-6 stimulation in $CD4^+$ T_{EM} cells (n=3). **(c)** Heatmap analysis of Affymetrix transcriptomic data identifies the top 20 genes (P<0.05; relative signal intensity of >150; 1.5-fold alteration) associated with protein tyrosine phosphatase enzyme family. Data is presented as a hierarchical cluster using the average linkage method (row 1-pearson rank correlation). Data are representative of two independent experiment (a,b) and one experiment involving biological replicates (c). ***P<0.001; ** P<0.01 (one-way ANOVA with Tukey's multiple comparison test (a) and two-way ANOVA with Sidak multiple comparison test (b). Data are shown as mean ± s.e.m (a) and mean ± s.d (b).

Figure 4. STAT1 activity is regulated by PTPN2. (**a**) Representative histogram of PTPN2 staining in $CD4^+$ T_N and $CD4^+$ T_{EM} cells by flow cytometry. (**b**) Flow cytometry analysis of STAT1 phosphorylation and PTPN2 expression in $CD4^+$ T_N and $CD4^+$ T_{EM} cells analyzed 30 min after stimulation with 20 ng/ml IL-6. (**c**) Immunohistochemistry of the inflamed synovium from wild-type mice with antigen-induced arthritis (day-10 post disease induction) in tissue sections stained with antibodies against CD3, Ptpn2 and pY-STAT1. Scale bar, 100µm (left panel) and 200µm (right panel). (**d**) Analysis of pY-STAT1 and pY-STAT3 in $CD4^+$ T_N and $CD4^+$ T_{EXP} cells derived from *Ptpn2*$^{fl/fl}$, Lck-Cre *Ptpn2*$^{fl/fl}$ (left panel) or wild-type and *Ptpn22*$^{-/-}$ mice (right panel) (n=4) exposed to IL-6 (20 ng/ml) for 30 min in combination with antibodies against CD3 and CD28. Fold change relative to the untreated controls are compared. (**e**) IL-21 and IL-17A quantification by flow cytometry in $CD4^+$ T_{EM} cells from *Ptpn2*$^{fl/fl}$ and Lck-Cre *Ptpn2*$^{fl/fl}$ mice (n=3). (f) ImageStream analysis of STAT1 and PTPN2 localization in $CD4^+$ T_N and $CD4^+$ T_{EM} cells stained with antibodies against STAT1, pY-STAT1, PTPN2 and CD4. Data are representative of three independent experiments (a,b), two independent experiments (f) and one experiment involving biological replicates (c,d,e). ****P<0.0001; *** P<0.001 (One-way ANOVA with Tukey's multiple comparison test (d) and Two-tailed unpaired Student's test (e). Data are shown as mean ± s.d.).

Figure 5. Transcriptomic analysis of IL-6 responses in CD4$^+$ T cells. (a) Circos visualisation details the IL-6 regulated gene changes in CD4$^+$ T_N and CD4$^+$ T_{EXP} cells (See *Supplemental Figure-2*), and *ex vivo* sorted CD4$^+$ T_{EM} cells. Total number of IL-6 regulated genes is presented in parenthesis for each population (*P*< 0.05, Chip Intensity 150+, and > 1.5-fold change). Lines coloured in red represent up-regulated genes and all down-regulated gene changes are blue. Connecting lines highlight common genes that are IL-6 regulated in two or more of the populations. **(b)** IPA analysis of genes associated with IL-6, STAT1 and STAT3 upstream regulators. Top left heat map shows the predicted activated state (orange) and the predicted inhibited state (blue) of transcription regulators. Upstream regulator analysis for CTLA4 and CD3 are presented as controls. Relative expression heat maps are presented as a hierarchical cluster using the average linkage method (row 1-pearson rank correlation). The differential expression of genes being regulated by IL-6, STAT1 or STAT3 is shown for CD4$^+$ T_N, CD4$^+$ T_{EXP} and CD4$^+$ T_{EM} cells. **(c)** IL-6 regulated gene changes derived from transcriptomic analysis were directly compared with datasets derived from IL-6 stimulated *Stat1*$^{-/-}$ and *Stat3*$^{-/-}$ CD4$^+$ T cells (GSE65621).

Figure 6. ChIP-seq analysis of STAT1 and STAT3 binding in IL-6 stimulated CD4$^+$ T cells. ChIP-seq was performed on genomic DNA extracted from sorted CD4$^+$ T_N and CD4$^+$ T_{EM} cells following 1-hour stimulation with IL-6 in presence of antibodies against CD3 and CD28. Peak calling and downstream data processing are described in *Materials & Methods*. **(a)** Pie charts show the proportion of peaks associated with STAT1 and STAT3 binding to defined genomic regions. The total number of peaks identified is displayed graphically. All datasets residing outside TSS regions were only included if located to exonic or intronic sites. **(b)** Analysis of gene clusters regulated by binding STAT1 and STAT3 in TSS promoter regions. The heat map shows the score value for each gene identified with Homer for STAT1 and STAT3 ChIP-seq data in CD4$^+$ T_N (blue) and CD4$^+$ T_{EM} (red) cells. **(c)** Comparison of ChIP-seq datasets against Affymetrix gene expression (relative significance; -(log10 (adjusted *P*-value)). Analysis of STAT1 and STAT3 datasets is shown for CD4$^+$ T_N (blue) and CD4$^+$ T_{EM} (red) subsets. An interactive figure of additional information can be found on-line (http://jones-cytokinelab.co.uk/NI2019/figure6c.shtml) **(d)** Circos visualization of STAT1 and STAT3 binding to TSS regions of genes under IL-6 regulation in CD4$^+$ T_N and CD4$^+$ T_{EM} cells. Connecting lines are color coded to reflect involvement of STAT1 (green), STAT3 (blue) or both STAT1 and STAT3 (orange).

Figure 7. IL-6 regulates the interaction of STAT1 and STAT3 with P300 enhancer sites. (a) Circos plot shows the co-localisation of STAT1 (blue) and STAT3 (orange) binding to genomic regions sharing P300 enrichment in CD4$^+$ T_N and CD4$^+$ T_{EM} cells. The connecting lines show the relationship of STAT1 and STAT3 binding between CD4$^+$ T_N and CD4$^+$ T_{EM} cells. P300 ChIP-seq datasets (Accession number GSE40463, GSE60482) are derived from T_H1, T_H2 and T_H17 cells. **(b)** Heat map showing the expression of all IL-6

644 regulated genes linked with P300 binding in $CD4^+$ T_N and $CD4^+$ T_{EM} cells (positioned left). The
645 correspondingly aligned heatmap (positioned right) shows the relationship to P300 sites in T_H1, T_H2 and
646 T_H17 cells and shows the number of clustered P300 sites affiliated to an individual gene (blue=0,
647 yellow=4). Specific examples of individual genes are shown. **(c)** Circos visualisation of 135 genes that
648 display P300 binding in association with either STAT1 or STAT3 in $CD4^+$ T_N versus $CD4^+$ T_{EM} cells. **(d)** IPA
649 predictions of the five distinct patterns of STAT binding identified from panel c. Hierarchical clustering of
650 canonical pathways was performed using -Log (*P*-value). *Supplemental Table 6* lists the canonical
651 pathways represented in the heatmap. **(e)** STAT1 binding enrichment quantification by ChIP-qPCR in
652 $Ptpn2^{fl/fl}$ and Lck-Cre:$Ptpn2^{fl/fl}$ $CD4^+$ T_{EM} cells (one experiment with pool samples from 12 *Ptpn2*$^{fl/fl}$ and 8
653 *Lck-Cre Ptpn2*$^{fl/fl}$ mice).
654
655 ***Figure 8.*** **Association of PTPN2 with rheumatoid arthritis. (a)** Correlations of *PTPN2* and *PTPN22* with
656 lymphocyte cell markers CD3 and CD20 (left). **(b)** Distribution of *PTPN2* and *PTPN22* in patients stratified
657 according synovial pathology (lymphoid – blue, myeloid – red and fibroid – green) (right). **(c)** Pearson
658 correlations of synovium *PTPN2* and *PTPN22* with inflammatory markers including *IL21*, *IL17A*, *CD274*
659 and *SOCS1* in lymphoid (blue), myeloid (red) and fibroid (green) phenotypes. *P* values were adjusted
660 using false discovery rate (FDR) correction (Benjamini-Hochberg).
661

Materials and methods-

Recombinant Cytokines- Recombinant mouse IL-6 (IL-6), IL-27, IL-10, IL-7 and IFNγ were purchased from R&D Systems. The IL-6-sIL-6R fusion protein HDS (Mw: 63.5kDa) was expressed in CHO cells and purified through a partnership with the CRO Biovian OY (Turku, Finland). HDS was engineered by coupling the entire coding sequence (amino acid residues 1-364) for the differentially-spliced variant of human IL-6R (containing the unique COOH-terminal amino acid sequence: GSRRRGSCGL) to IL-6 (amino acid residues 29-212) *via* a flexible glycine-serine rich linker sequence (single amino sequence: GGGGSGGGGSLE)[8].

Antibodies- Mouse specific antibodies against CD3ε/γ (17A2; Biolegend), CD4 (RM4-5; eBioscience), CD25 (PC61.5; eBioscience), CD44 (IM7; BD Biosciences), CD62L (MEL-14; Life Technologies), CD126 (D7715A7; eBioscience), CD127 (25-1271-82; eBioscience), βTCR (H57-597), gp130 (125623; R&D Systems), IFNγ (XMG1.2; eBioscience), IL-4 (11B11; eBioscience), IL-17A (TC11-18H10.1; Biolegend), IL-21 (Recombinant mouse IL-21R Fc Chimera protein; R&D and IL-21 receptor antibody; Jackson Immuno Research) and PTPN2 (AF1930; R&D) were used. For detection of human antigens, we used antibodies specific to CD3 (UCHT1; BioLegend), CD4 (RPA-T4; eBioscience), CD45RA (HI100; BioLegend), CD45RO (UCHL1; BioLegend), CD62L (DREG-56; BD Biosciences), CD197 (CCR7; G043H7; BioLegend). Human and mouse cross-specific antibodies to pY-STAT1 (pY701; 4a), pY-STAT3 (pY705; 4/P-STAT3), pS-STAT1 (pS727; K51-856) and pS-STAT3 (pS727, 49/p-Stat3) were from BD Biosciences.

Mice- Inbred wild type C57BL/6 male mice were purchased from Charles River UK. C57BL/6 IL-6 receptor deficient mice (*Cd126*$^{-/-}$) mice have been described previously and were bred under approved UK Home Office guidelines in Cardiff University[7]. *Ptpn2*$^{fl/fl}$*, Lck-Cre:Ptpn2*$^{fl/fl}$*,* and *Ptpn22*$^{-/-}$ mice were bred and housed at the Peter MacCallum Cancer Centre (Melbourne, Australia). All mice were 8-12 weeks of age. For T cell stimulation experiments eight-week-old male *Lck*-Cre;*Ptpn2*$^{fl/fl}$ mice and *Ptpn2*$^{fl/fl}$ littermate controls were used[38]. All procedures were performed in accordance with the NHMRC Australian Code of Practice for the Care and Use of Animals, and approved by the Peter MacCallum Animal Ethics and Experimentation Committee (Ethics number: AEEC 570). Antigen-induced arthritis was performed under the UK Home Office-approved project licences PPL 30/2928 and PB3E4EE13 as previously described[51]. Briefly, mice were immunized (s.c.) with 100 µl mBSA (1 mg/ml emulsified in Complete Freund's Adjuvant; CFA) and 160 ng *Bordetella pertussis* toxin (i.p.) (all from Sigma-Aldrich). Mice were administered with mBSA and CFA (s.c.) one week later. Inflammatory arthritis was triggered 21 days following the initial immunization by intra-articular administration of mBSA (10 µl; 10 mg/ml) into the right knee joint. Animals were monitored daily for wellbeing and clinical signs of arthritis, and killed at indicated time points for evaluation of joint-infiltrating T cells by flow cytometry and immunofluorescence. For flow cytometric analysis of synovial $CD4^+$ T cells, inflamed synovium was first

dissected and digested in Collagenase type IV (37˚C, 1 hour) before passing through a 40µm cell strainer to generate single cell suspensions.

Human synovial samples- Synovial samples were acquired through a minimally invasive ultrasound-guided synovial biopsy (see Reference[52]) from 87 patients presenting with early rheumatoid arthritis (RA) naïve to therapy from the Pathobiology of Early Arthritis Cohort (PEAC). Ethical approval was granted by the King's College Hospital Research Ethics Committee (REC 05/Q0703/198). Paraffin embedded sections (3µm) of each biopsy was stained with haematoxylin and eosin. Immune cell infiltration was determined in sequentially cut sections by staining for B-cells (CD20), T cells (CD3), macrophages (CD68) and plasma cells (CD138) as previously reported, categorising samples into Lympho-myeloid, Diffuse-Myeloid and Pauci-immune Fibroid pathotypes[53].

$CD4^+$ T cell cultures- Murine $CD4^+$ T cells were enriched by negative magnetic selection (Miltenyi Biotec) before purification of naïve ($CD4^+CD25^-CD44^{lo}CD62L^{hi}CD127^{hi}$), central memory ($CD4^+CD25^-CD44^{hi}CD62L^{hi}CD127^{hi}$), effector ($CD4^+CD25^-CD44^{lo}CD62L^{lo}CD127^{lo\text{-}int}$) or effector memory ($CD4^+CD25^-CD44^{hi}CD62L^{lo}CD127^{int\text{-}hi}$) T cells using a BD FACS ARIA II (BD Biosciences). T cell subset purity was >98%. Naïve $CD4^+$ T cells were cultured in RPMI-1640 supplemented with 10% (v/v) FCS, 2mM L-glutamine, 100U/ml penicillin, 100µg/ml streptomycin, 1mM sodium pyruvate and 50µM 2-mercaptoethanol. 1 x 10^5 CD4 T cells were activated by plate bound anti-CD3 (1µg/ml; 145-2C11, R&D Systems) and soluble anti-CD28 (5µg/ml; 37.51, eBioscience). Where indicated, $CD4^+$ T cells were rested for 48 hours in the absence of stimulatory antibodies or cytokines (see Supplementary Fig. 2a). $CD4^+$ T cells from the inguinal lymph nodes of mBSA-immunized and non-immunized mice were derived using a $CD4^+$ T cell isolation kit (Miltenyi Biotec) and treated with IL-6 for 30 min with anti-CD3/CD28 stimulation. Human peripheral blood mononuclear cells (PBMC) were isolated from fresh whole blood as previously described[54]. Naïve ($CD3^+CD4^+CD45RO^{lo}CD62L^{hi}CCR7^{hi}$), central memory ($CD3^+CD4^+CD45RO^{hi}CD62L^{hi}CCR7^{hi}$), effector ($CD3^+CD4^+CD45RO^{lo}CD62L^{lo}CCR7^{lo}$) or effector memory ($CD3^+CD4^+CD45RO^{hi}CD62L^{lo}CCR7^{lo}$) $CD4^+$ T cells were then purified using a BD FACS ARIA II (BD Biosciences). To investigate the involvement of protein tyrosine phosphatases CD4 T cells were pre-treated (5 min) with 5mM sodium orthovanadate (New England BioLabs (UK) Ltd) prior to subsequent stimulation.

Histological analysis- Formalin-fixed paraffin-embedded knee joints from AIA-challenged mice were prepared for immunofluorescent and immunohistochemical detection of antigens as described previously[51]. For immunofluorescence, sections were rehydrated and antigen retrieval performed in 10mM sodium citrate buffer containing 0.05% (v:v) Tween 20 (95°C, 40 min). Sections were incubated with 10% (v:v) goat or swine serum appropriate to the secondary antibody. Cells positive for CD3 and

intracellular phospho-STAT1 and STAT3 were detected using CD3 (A0452, Dako), and pY-STAT1 (Tyr701; 58D6) or pY-STAT3 (Tyr705; D3A7) specific antibodies from Cell Signaling Technologies. For CD3 staining, primary antibody detection was performed using biotinylated swine anti-rabbit IgG (E0431, Dako) with streptavidin-APC (BD Biosciences). For pY-STAT1 and pY-STAT3 detection a secondary rabbit anti-goat IgG Alexa Fluor 488 antibody (Life Technologies) was used. Slides were mounted with Prolong Gold Antifade with DAPI nuclear counterstain (Invitrogen). Images were collected using a Zeiss Apotome microscope and analyzed using ImageJ software. For immunohistochemistry, antigens were detected in paraffin sections using antibodies against CD3 (A0452, Dako), pY-STAT1 (Tyr701; 58D6) and PTPN2 (AF1930, R&D Systems). Antigen retrieval was performed as above, and endogenous peroxidase activity blocked using 3% (v:v) H_2O_2. Antibody labelling was detected using biotinylated secondary antibodies (Dako, E0431), the Vectastain ABC kit and diaminobenzidine (Vector Laboratories). Sections were counterstained with haematoxylin. Images were collected using Leica DM 2000 Led and quantification of staining performed using the Leica QWin microscope imaging software.

Flow cytometry- Analysis was performed as described previously[7, 8, 15]. For the intracellular detection of STAT1 and STAT3 phosphorylation, purified $CD4^+$ T cells were fixed in 2% (w:v) paraformaldehyde for 15 min at 37^{o}C, followed by permeabilization in 90% (v:v) methanol at -20^{o}C for 3hrs. Cells were stained for CD4 and phosphorylated STAT1, STAT3 [7]. To evaluate effector cytokine production, $CD4^+$ T cells were stimulated with 50ng PMA (phorbol 12-Myristate 13-Acetate), 500ng ionomycin and 3µM monesin for 4 hours prior to flow cytometric analysis[7, 8, 15]. Cells were acquired on a CyAn ADP analyzer (Beckman-Coulter) and analysed using Summit (software v4.3, Beckman-Coulter) or FlowJo 10 (TreeStar). For imaging flow cytometry, cells were resuspended in 100 µl of PBS and acquired using the ImageStream imaging flow cytometer (Amnis). For co-localization analysis ImageStream software IDEAS (Amnis) was used.

RNA purification and Q-PCR- For quantitative real-time PCR (Q-PCR), and Affymetrix gene chip analysis, total RNA was extracted from purified or cultured CD4 T cells using the RNeasy Mini Kit (Qiagen) and QIAshredders (Qiagen). Contaminating genomic DNA was removed by on-column DNase digestion (Qiagen). RNA was converted to cDNA using the High Capacity cDNA Reverse Transcription Kit with RNase Inhibitor kit (Life Technologies). Gene expression was determined by Q-PCR[8, 55] using the QuantStudio 12K Flex Real-Time PCR system and the following TaqMan probes from Thermofisher: *Ahr* (Mm00478932_m1), *Bcl3* (Mm00504306_m1), *Bcl6* (Mm01342164_m1), *Il10* (Mm00439614_m1), *Il21* (Mm00517640_m1), *Irf1* (Mm01288580_m1), *Socs3* (Mm00545913_s1), *Stat3* (Mm01219775_m1), *Pim1* (Mm00435712_m1) and *Actb* (Mm01205647_g1) as a housekeeping gene. Relative mRNA expression was determined by the comparative cycle threshold (CT) method and normalised to the gene *Actb*.

Affymetrix microarray and transcriptomic analysis- Purification of high quality RNA (RNA integrity number >8.5) was confirmed using Agilent RNA Nano microfluidic chips using a 2100 Bioanalyzer Instrument (Agilent Technologies). Expression profiling was performed in triplicate using Affymetrix Mouse GeneChip® 2.0ST microarrays (Affymetrix). Single-stranded cDNA was synthesized using the Ambion® WT (Whole Transcript) Expression Kit with the Affymetrix® Genechip® Poly-A RNA Control Kit and Terminal Labelling kit. Arrays were scanned using the GeneChip Scanner 3000 7G (Affymetrix). Raw Affymetrix data files (CEL files) were imported into an in-house analysis pipeline written in R (version 3.1.1) using Bioconductor packages, namely limma, affy and oligo[56, 57, 58, 59]. Data were background corrected, log2 transformed and quantile normalized using the oligo package (RMA) "best practice". Differentially expressed genes and transcripts were identified using the limma package "best practice" workflow and *P*-values were corrected by multiple testing using Benjamini-Hochberg (false discovery rate)[57].

Bespoke coding (Perl) (Code available on request) was used to unite data over all conditions. To identify differentially expressed genes over all experiments, we selected the genes that were classified as having altered expression (either decreasing or decreasing) by a difference of 1.5-fold or greater, with a significant value $P \leq 0.05$ and a minimal expression value of 150 relative intensity units. Only transcripts fulfilling all these selection criteria in three independent microarray experiments were included in the analysis. Files were also created in the input format required for molecular and pathway analysis using Metacore integrated software suite (Thomson Reuters)[59] and Ingenuity Pathway Analysis (IPA, http://www.ingenuity.com/products/ipa). Transcriptome matrix visualization and hierarchical clustering were performed using Morpheus software (https://software.broadinstitute.org/morpheus/). Circos plot were obtained using the Circos software (http://circos.ca/software/)[60]. Networks were visualization and analysed using the open sourced program Gephi (0.9.1) (https://gephi.org/)**.** Microarray data have been deposited in ArrayExpress under Accession code E-MTAB-7682.

RNA-sequencing- Open access datasets from IL-6 treated $Stat1^{-/-}$ and $Stat3^{-/-}$ T cells (GSE65621) were obtained from GEO (https://www.ncbi.nlm.nih.gov/geo/) and aligned and processed using an in-house bioinformatic pipeline. Briefly, RNA-seq single-end fastq files were mapped to mouse assembly GRCm38 using STAR[61]. Transcript counts were produced with FeatureCounts[62] and data normalised using the Bioconductor package, DeSeq2[63] obtaining gene expression values as FPKM (Fragments Per Kilobase Million).

For the human samples, RNA from homogenised synovial tissue was extracted in Trizol. 1µg total RNA was used as input material for library preparation using TruSeq RNA Sample Preparation Kit v2 (Illumina). Generated libraries were amplified with 10 cycles of PCR. Library size was confirmed using 2200

TapeStation and High Sensitivity D1K screen tape (Agilent Technologies) and concentration was determined by Q-PCR based method using Library quantification kit (KAPA). Libraries were multiplexed (five per lane) and sequenced on Illumina HiSeq2500 (Illumina) to generate 50 million paired-end 75 base pair reads. Transcript abundance was derived using Kallisto v0.43.0 with GENCODE v24/GRCh38 as reference[64]. Transcript abundances were summarised over transcript isoforms using Bioconductor package tximport 1.4.0. Imported abundances were processed using DESeq2 1.14.1 and transformed as regularised log expression (RLE). Statistical analysis of gene-gene correlations was performed using Pearson correlation. P values were adjusted using false discovery rate (FDR) correction (Benjamini-Hochberg). RNA-seq data have been deposited in ArrayExpress under Accession code E-MTAB-6141.

Chromatin Immunoprecipitation (ChIP)-seq- STAT1 and STAT3 chromatin Immunoprecipitation was performed as previously described[20]. Briefly, $1x10^7$ naïve (T_N) and effector memory (T_{EM}) $CD4^+$ T cells were activated for 1h with 20ng/ml IL-6 in the presence of antibodies against CD3 and CD28 (as described earlier). Genomic DNA was extracted, cross-linked and fragmented by sonication prior to overnight incubation with 5ug of anti-STAT1 (sc-592, Santa Cruz Biotechnology) or anti-STAT3 (sc-482, Santa Cruz Biotechnology) antibodies. The quality of the immunoprecipitation was confirmed by ChIP-qPCR for *Irf1* and *Socs3*. To minimize systematic biases in the downstream data, an input reference control sample (chromatin taken before ChIP) was used to correct for genomic copy number variations, sonication-induced fragmentation bias, and chromatin accessibility. ChIP-seq libraries for Ion Torrent sequencing were prepared according to manufacturer's instructions (# 4473623, Ion ChIP-Seq Library Preparation on the Ion Proton TM System). Briefly, DNA fragments were end-repaired and ligated to ion-compatible adapters. Libraries were amplified and size-selected for insert lengths of approximately 100-250bp. Between 40M to 70M reads were obtained for each sample and mapped to Murine Genome Build GRCm38 (mm10) using the Ion Proton recommended mapper, Bowtie2[65, 66]. Reads were removed where mapping quality was less than q20 (phred score) and peaks called using HOMER (Hypergeometric Optimization of Motif EnRichment). To identify putative peaks in both ChIP and input, we first used HOMER findPeaks with a False Discovery Rate (FDR) value of 0.05. To identify sample peaks in the context of input, we then used HOMER findPeaks with the default parameters (Fold Change > 4-fold, *P*-value < 0.0001). Peaks were visualised using Integrative Genomics Viewer (IGV 2.3.88[67]). Available p300 ChIP-seq fastq files from $CD4^+$ T cells, T_H1, T_H2 (GSE40463) and T_H17 (GSE60482) were obtained from GEO (https://www.ncbi.nlm.nih.gov/geo/) and aligned and processed using an in-house pipeline. Reads were mapped to the same *mm10* assembly using BWA. All reads with a mapping quality less than q20 were removed. HOMER [i]software was used to locate P300 enhancer elements (using the Homer option, –style super) and parameters Fold Change > 2-fold, *P*-value < 0.0001. To align STAT1 or STAT3 peaks with SE regions, overlapping loci identified by STAT1 and STAT3 ChIP-seq and p300 ChIP-seq were identified

using bedtools (http://bedtools.readthedocs.io/en/latest/)[68]. ChIP-Seq data have been deposited in ArrayExpress under Accession code E-MTAB-6273.

ChIP-qPCR- To validate STAT-binding to promoter regions, Taqman custom assays were designed (see Supplementary Table 2 for oligonucleotide primer sequences) and qPCR performed using a QuantStudio 12K Flex Real-Time PCR System. For analysis of SP1, chromatin immunoprecipitation was conducted as previously described using 5ug of SP1 antibody (#17-601, Millipore) or isotype specific IgG control. Analysis by qPCR used oligonucleotide primer sequences to the promoter regions of *Irf1*, *Socs3, Stat3, Cd274, Il4ra, Junb* and *Socs1* (Supplementary Table 2). Specific enrichment was normalised by subtracting the IgG control values from those derived for the input and antibody specific immunoprecipitation samples. Value were expressed as $2^{\wedge\Delta CT}$.

Motif finding- MEME Suite 4.11.2 software was used to discover *de novo* enriched DNA consensus sequences present in peaks identified within the STAT1 or STAT3 ChIP-seq datasets. All sequence predictions derived from MEME based on the interaction of known transcription factors with target DNA sequences where substantiated using STAMP[69] (http://benoslab.pitt.edu/stamp/) and JASPAR database (http://jaspar.genereg.net/cgi-bin/jaspar_db.pl)[70].

Statistics- To determine the statistical significance of differences between data sets, Two-tailed unpaired Student's t-test were performed when two populations were compared. One-way ANOVA followed Tukey's comparison test was used for multiple comparisons, unless otherwise specified, conducted using GraphPad Prism 5 (GraphPad Software). Statistical significance is also highlighted with the following notations: **P*<0.05; ***P*<0.01; ****P*<0.001, *****P*<0.0001. $P \leq 0.05$ was considered significantly different.

Reporting Summary- Further information on experimental design is available in the *Life Sciences Reporting Summary* linked to this article.

Data Availability- Microarray, ChiP-seq and RNA-seq data have been deposited in ArrayExpress under Accession code E-MTAB-7682, E-MTAB-6273 and E-MTAB-6141, respectively. Available p300 ChIP-seq fastq files from CD4 T cells, Th1, Th2 (GSE40463) and Th17 (GSE60482), and $Stat1^{-/-}$ and $Stat3^{-/-}$ T cells (GSE65621) were obtained from GEO (https://www.ncbi.nlm.nih.gov/geo/). Access to interactive data sets can be found at www.jones-cytokinelab.co.uk (see relevant *Figure Legends* for additional information).

References

51. Jones, G.W. *et al.* Interleukin-27 inhibits ectopic lymphoid-like structure development in early inflammatory arthritis. *J Exp Med* **212**, 1793-1802 (2015).

52. Kelly, S. *et al.* Ultrasound-guided synovial biopsy: a safe, well-tolerated and reliable technique for obtaining high-quality synovial tissue from both large and small joints in early arthritis patients. *Ann Rheum Dis* **74**, 611-617 (2015).

53. Humby, F. *et al.* Ectopic lymphoid structures support ongoing production of class-switched autoantibodies in rheumatoid synovium. *PLoS medicine* **6**, e1 (2009).

54. Jones, G.W. *et al.* Naive and activated T cells display differential responsiveness to TL1A that affects Th17 generation, maintenance, and proliferation. *FASEB J* **25**, 409-419 (2011).

55. Greenhill, C.J. *et al.* Interleukin-10 regulates the inflammasome-driven augmentation of inflammatory arthritis and joint destruction. *Arthritis Res Ther* **16**, 419 (2014).

56. Gentleman, R.C. *et al.* Bioconductor: open software development for computational biology and bioinformatics. *Genome Biol* **5**, R80 (2004).

57. Ritchie, M.E. *et al.* limma powers differential expression analyses for RNA-sequencing and microarray studies. *Nucleic Acids Res* **43**, e47 (2015).

58. Gautier, L., Cope, L., Bolstad, B.M. & Irizarry, R.A. affy--analysis of Affymetrix GeneChip data at the probe level. *Bioinformatics* **20**, 307-315 (2004).

59. Carvalho, B.S. & Irizarry, R.A. A framework for oligonucleotide microarray preprocessing. *Bioinformatics* **26**, 2363-2367 (2010).

60. Krzywinski, M. *et al.* Circos: an information aesthetic for comparative genomics. *Genome Res* **19**, 1639-1645 (2009).

61. Dobin, A. *et al.* STAR: ultrafast universal RNA-seq aligner. *Bioinformatics* **29**, 15-21 (2013).

62. Liao, Y., Smyth, G.K. & Shi, W. featureCounts: an efficient general purpose program for assigning sequence reads to genomic features. *Bioinformatics* **30**, 923-930 (2014).

63. Love, M.I., Huber, W. & Anders, S. Moderated estimation of fold change and dispersion for RNA-seq data with DESeq2. *Genome Biol* **15**, 550 (2014).

64. Bray, N.L., Pimentel, H., Melsted, P. & Pachter, L. Near-optimal probabilistic RNA-seq quantification. *Nature biotechnology* **34**, 525-527 (2016).

65. Langmead, B. & Salzberg, S.L. Fast gapped-read alignment with Bowtie 2. *Nat Methods* **9**, 357-359 (2012).

66. Robertson, G. *et al.* Genome-wide profiles of STAT1 DNA association using chromatin immunoprecipitation and massively parallel sequencing. *Nat Methods* **4**, 651-657 (2007).

67. Robinson, J.T. *et al.* Integrative genomics viewer. *Nature biotechnology* **29**, 24-26 (2011).

68. Quinlan, A.R. & Hall, I.M. BEDTools: a flexible suite of utilities for comparing genomic features. *Bioinformatics* **26**, 841-842 (2010).

69. Mahony, S. & Benos, P.V. STAMP: a web tool for exploring DNA-binding motif similarities. *Nucleic Acids Res* **35**, W253-258 (2007).

70. Mathelier, A. *et al.* JASPAR 2016: a major expansion and update of the open-access database of transcription factor binding profiles. *Nucleic Acids Res* **44**, D110-115 (2016).

918

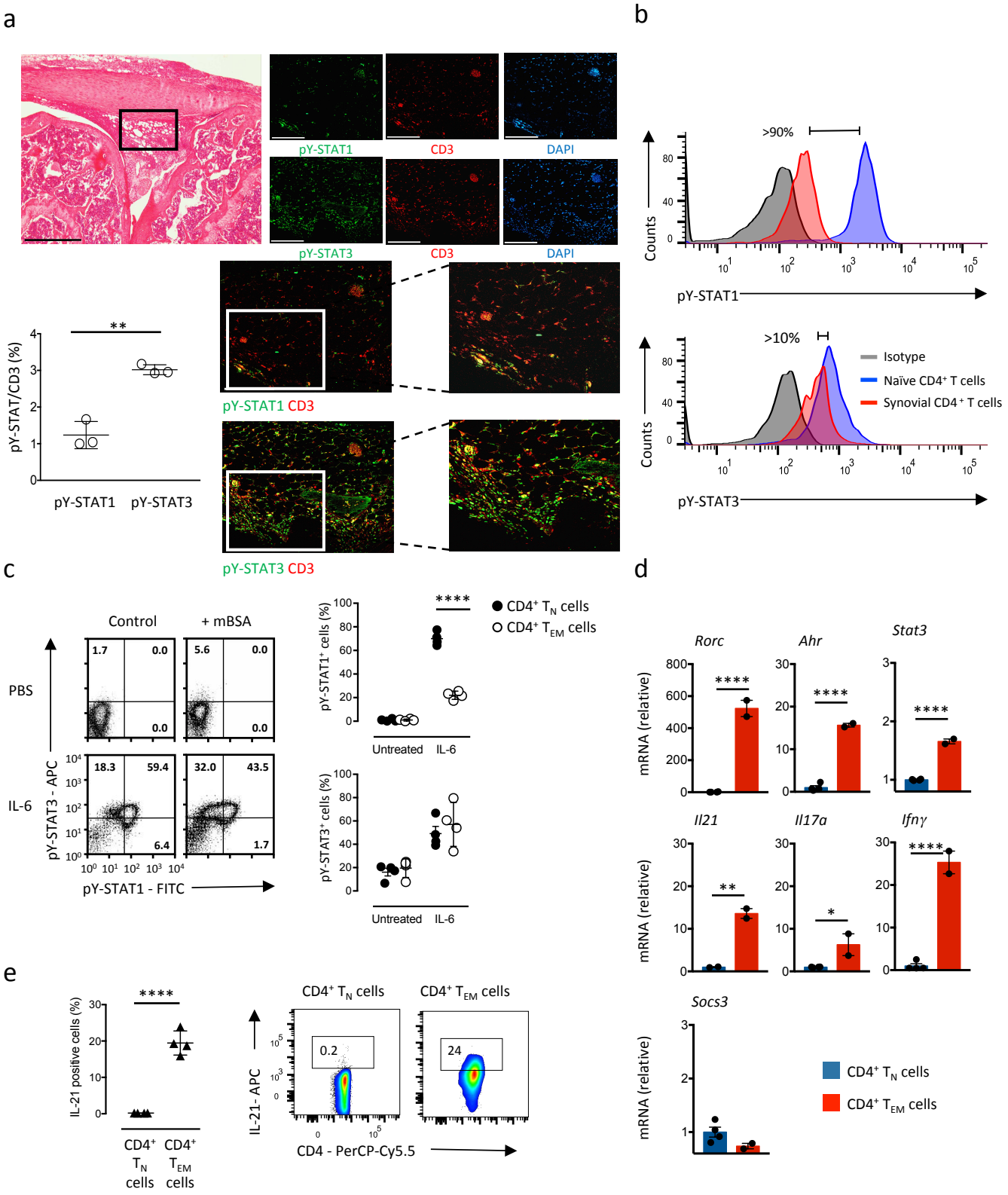
a
pY-STAT1
CD3
DAPI
pY-STAT3
CD3
DAPI
pY-STAT1 CD3
pY-STAT3 CD3
pY-STAT/CD3 (%)
**
pY-STAT1
pY-STAT3
b
>90%
Counts
pY-STAT1
>10%
Isotype
Naïve CD4+ T cells
Synovial CD4+ T cells
Counts
pY-STAT3
c
Control
+ mBSA
PBS
IL-6
1.7
0.0
0.0
5.6
0.0
0.0
18.3
59.4
6.4
32.0
43.5
1.7
pY-STAT3 - APC
pY-STAT1 - FITC
****
CD4+ TN cells
CD4+ TEM cells
pY-STAT1+ cells (%)
Untreated
IL-6
pY-STAT3+ cells (%)
Untreated
IL-6
d
Rorc
Ahr
Stat3
Il21
Il17a
Ifnγ
Socs3
mRNA (relative)
****
**
*
CD4+ TN cells
CD4+ TEM cells
e
IL-21 positive cells (%)
****
CD4+ TN cells
CD4+ TEM cells
CD4+ TN cells
CD4+ TEM cells
0.2
24
IL-21- APC
CD4 - PerCP-Cy5.5

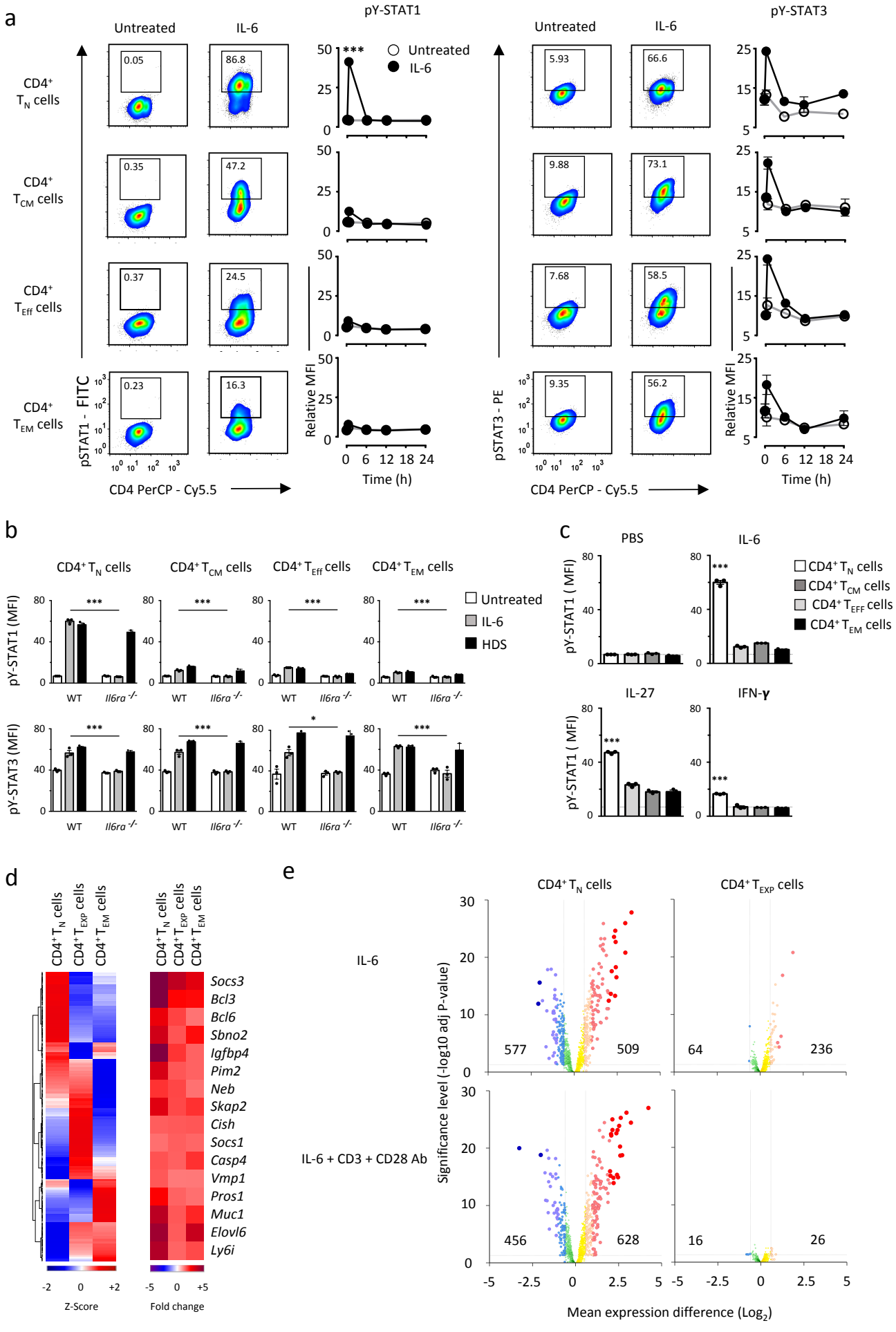
a
Untreated
IL-6
pY-STAT1
pY-STAT3
CD4+ TN cells
CD4+ TCM cells
CD4+ TEff cells
CD4+ TEM cells
0.05
86.8
0.35
47.2
0.37
24.5
0.23
16.3
5.93
66.6
9.88
73.1
7.68
58.5
9.35
56.2
***
Untreated
IL-6
Relative MFI
Time (h)
pSTAT1 - FITC
pSTAT3 - PE
CD4 PerCP - Cy5.5
b
CD4+ TN cells
CD4+ TCM cells
CD4+ TEff cells
CD4+ TEM cells
pY-STAT1 (MFI)
pY-STAT3 (MFI)
Untreated
IL-6
HDS
WT
Il6ra -/-
c
PBS
IL-6
IL-27
IFN-γ
pY-STAT1 (MFI)
CD4+ TN cells
CD4+ TCM cells
CD4+ TEFF cells
CD4+ TEM cells
d
CD4+ TN cells
CD4+ TEXP cells
CD4+ TEM cells
Socs3
Bcl3
Bcl6
Sbno2
Igfbp4
Pim2
Neb
Skap2
Cish
Socs1
Casp4
Vmp1
Pros1
Muc1
Elovl6
Ly6i
Z-Score
Fold change
e
IL-6
IL-6 + CD3 + CD28 Ab
CD4+ TN cells
CD4+ TEXP cells
577
509
64
236
456
628
16
26
Significance level (-log10 adj P-value)
Mean expression difference (Log2)

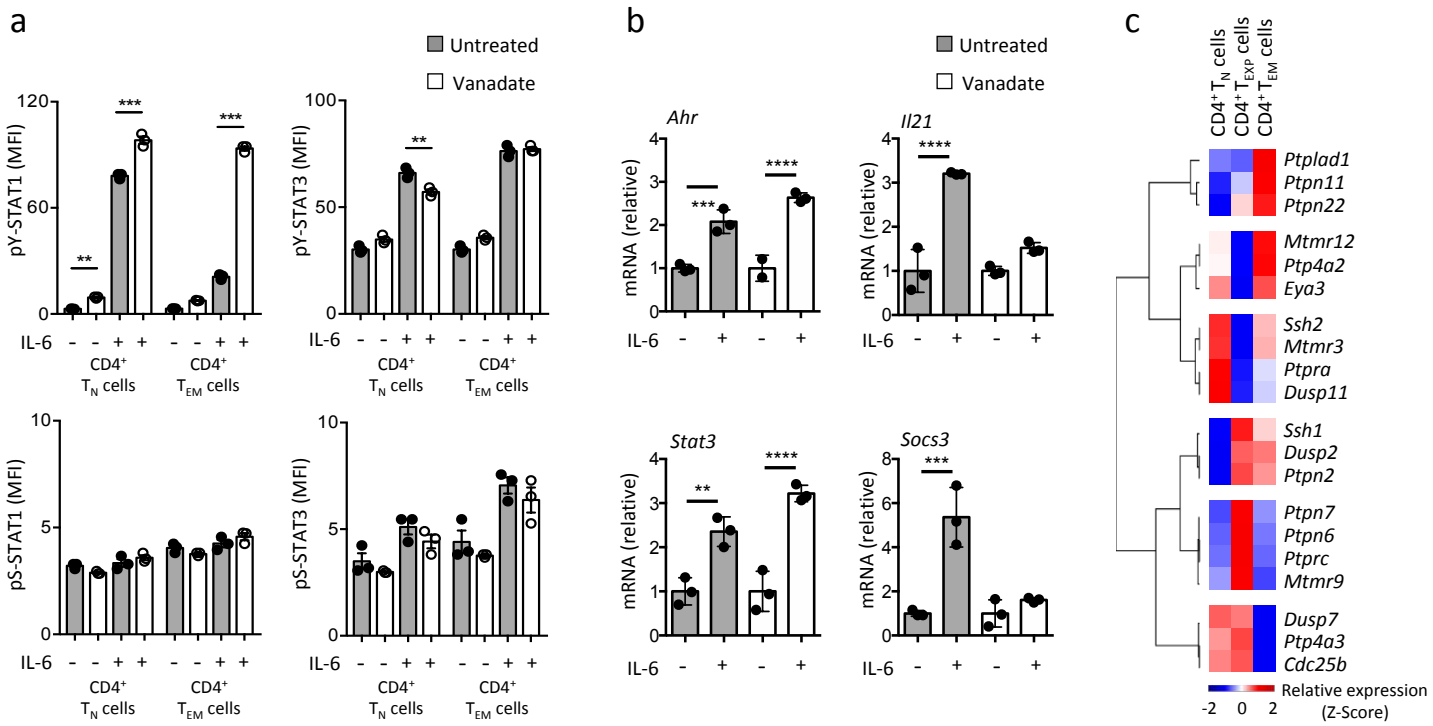
a
Untreated
Vanadate
pY-STAT1 (MFI)
pY-STAT3 (MFI)
pS-STAT1 (MFI)
pS-STAT3 (MFI)
IL-6
CD4+ TN cells
CD4+ TEM cells
b
Ahr
Il21
Stat3
Socs3
mRNA (relative)
c
CD4+ TN cells
CD4+ TEXP cells
CD4+ TEM cells
Ptplad1
Ptpn11
Ptpn22
Mtmr12
Ptp4a2
Eya3
Ssh2
Mtmr3
Ptpra
Dusp11
Ssh1
Dusp2
Ptpn2
Ptpn7
Ptpn6
Ptprc
Mtmr9
Dusp7
Ptp4a3
Cdc25b
Relative expression
(Z-Score)

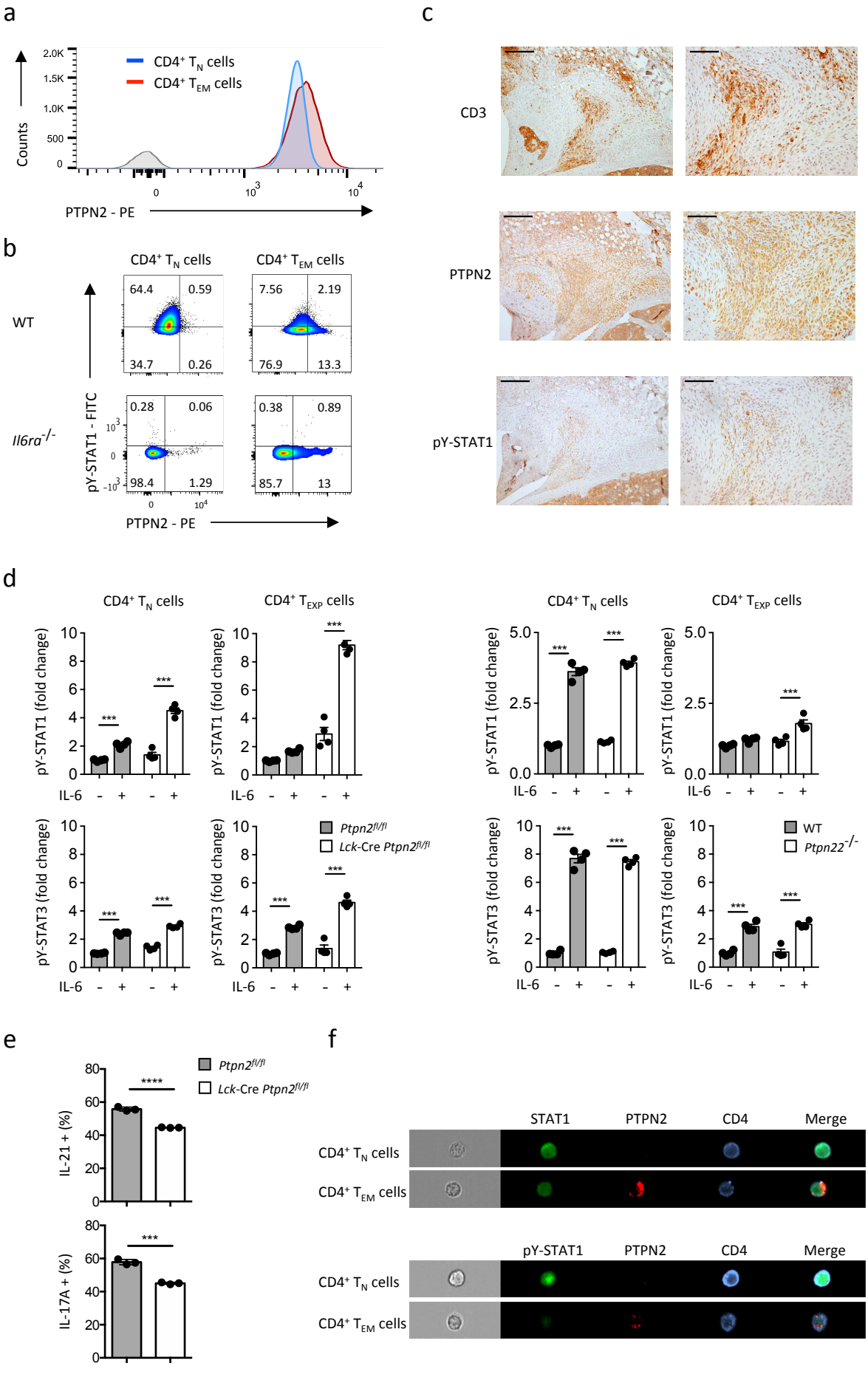
a
CD4+ TN cells
CD4+ TEM cells
Counts
PTPN2 - PE
b
CD4+ TN cells
CD4+ TEM cells
WT
Il6ra-/-
64.4
0.59
34.7
0.26
7.56
2.19
76.9
13.3
0.28
0.06
98.4
1.29
0.38
0.89
85.7
13
pY-STAT1 - FITC
PTPN2 - PE
c
CD3
PTPN2
pY-STAT1
d
CD4+ TN cells
CD4+ TEXP cells
pY-STAT1 (fold change)
pY-STAT3 (fold change)
IL-6
Ptpn2fl/fl
Lck-Cre Ptpn2fl/fl
WT
Ptpn22-/-
e
Ptpn2fl/fl
Lck-Cre Ptpn2fl/fl
IL-21 + (%)
IL-17A + (%)
f
STAT1
PTPN2
CD4
Merge
CD4+ TN cells
CD4+ TEM cells
pY-STAT1

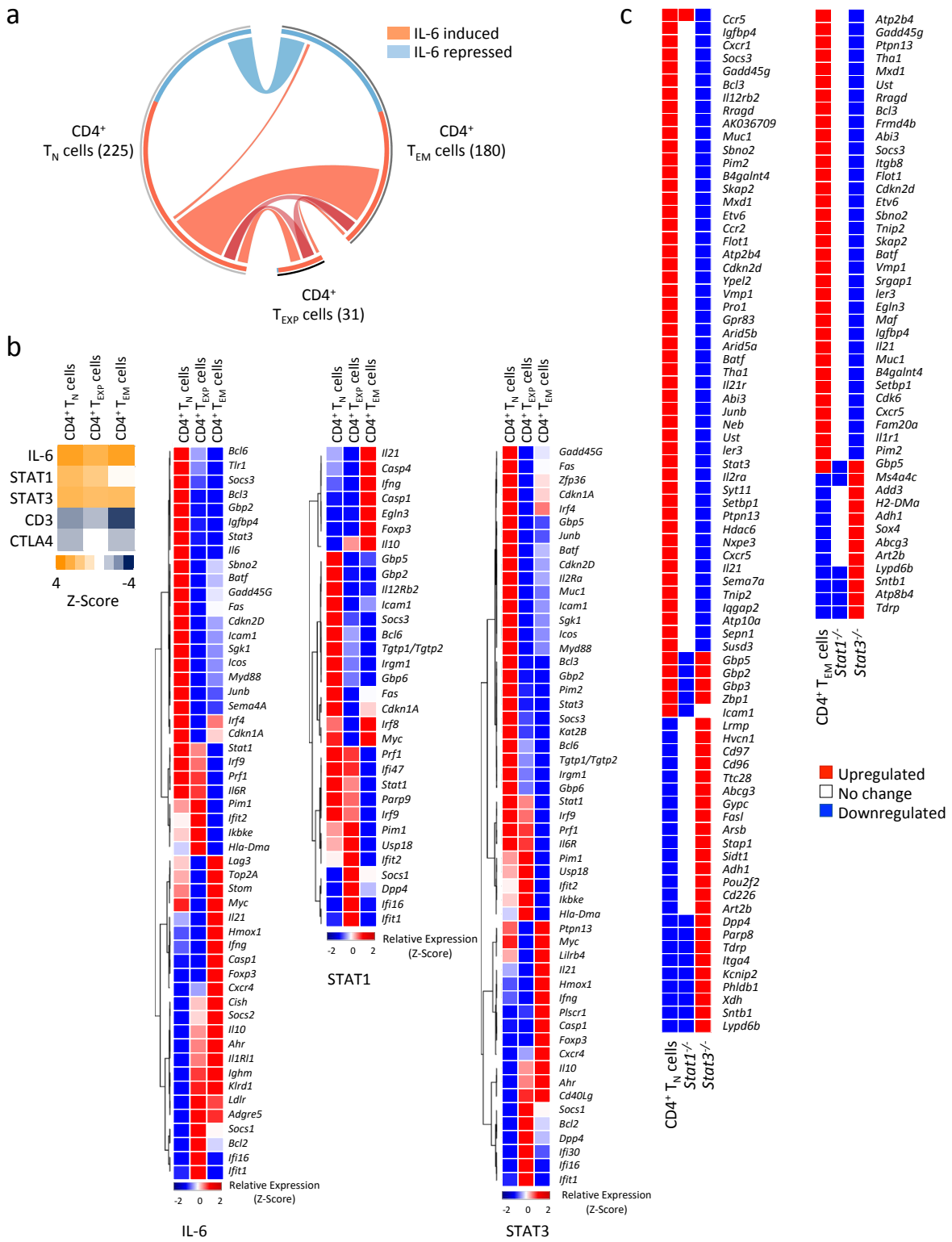
a
IL-6 induced
IL-6 repressed
CD4+ T_N cells (225)
CD4+ T_EM cells (180)
CD4+ T_EXP cells (31)
b
CD4+ T_N cells
CD4+ T_EXP cells
CD4+ T_EM cells
IL-6
STAT1
STAT3
CD3
CTLA4
4
-4
Z-Score
Bcl6 Tlr1 Socs3 Bcl3 Gbp2 Igfbp4 Stat3 Il6 Sbno2 Batf Gadd45G Fas Cdkn2D Icam1 Sgk1 Icos Myd88 Junb Sema4A Irf4 Cdkn1A Stat1 Irf9 Prf1 Il6R Pim1 Ifit2 Ikbke Hla-Dma Lag3 Top2A Stom Myc Il21 Hmox1 Ifng Casp1 Foxp3 Cxcr4 Cish Socs2 Il10 Ahr Il1Rl1 Ighm Klrd1 Ldlr Adgre5 Socs1 Bcl2 Ifi16 Ifit1
Relative Expression (Z-Score)
-2 0 2
IL-6
Il21 Casp4 Ifng Casp1 Egln3 Foxp3 Il10 Gbp5 Gbp2 Il12Rb2 Icam1 Socs3 Bcl6 Tgtp1/Tgtp2 Irgm1 Gbp6 Fas Cdkn1A Irf8 Myc Prf1 Ifi47 Stat1 Parp9 Irf9 Pim1 Usp18 Ifit2 Socs1 Dpp4 Ifi16 Ifit1
Relative Expression (Z-Score)
-2 0 2
STAT1
Gadd45G Fas Zfp36 Cdkn1A Irf4 Gbp5 Junb Batf Cdkn2D Il2Ra Muc1 Icam1 Sgk1 Icos Myd88 Bcl3 Gbp2 Pim2 Stat3 Socs3 Kat2B Bcl6 Tgtp1/Tgtp2 Irgm1 Gbp6 Stat1 Irf9 Prf1 Il6R Pim1 Usp18 Ifit2 Ikbke Hla-Dma Ptpn13 Myc Lilrb4 Il21 Hmox1 Ifng Plscr1 Casp1 Foxp3 Cxcr4 Il10 Ahr Cd40Lg Socs1 Bcl2 Dpp4 Ifi30 Ifi16 Ifit1
Relative Expression (Z-Score)
-2 0 2
STAT3
c
Ccr5 Igfbp4 Cxcr1 Socs3 Gadd45g Bcl3 Il12rb2 Rragd AK036709 Muc1 Sbno2 Pim2 B4galnt4 Skap2 Mxd1 Etv6 Ccr2 Flot1 Atp2b4 Cdkn2d Ypel2 Vmp1 Pro1 Gpr83 Arid5b Arid5a Batf Tha1 Il21r Abi3 Junb Neb Ust Ier3 Stat3 Il2ra Syt11 Setbp1 Ptpn13 Hdac6 Nxpe3 Cxcr5 Il21 Sema7a Tnip2 Iqgap2 Atp10a Sepn1 Susd3 Gbp5 Gbp2 Gbp3 Zbp1 Icam1 Lrmp Hvcn1 Cd97 Cd96 Ttc28 Abcg3 Gypc Fasl Arsb Stap1 Sidt1 Adh1 Pou2f2 Cd226 Art2b Dpp4 Parp8 Tdrp Itga4 Kcnip2 Phldb1 Xdh Sntb1 Lypd6b
CD4+ T_N cells
Stat1-/-
Stat3-/-
Atp2b4 Gadd45g Ptpn13 Tha1 Mxd1 Ust Rragd Bcl3 Frmd4b Abi3 Socs3 Itgb8 Flot1 Cdkn2d Etv6 Sbno2 Tnip2 Skap2 Batf Vmp1 Srgap1 Ier3 Egln3 Maf Igfbp4 Il21 Muc1 B4galnt4 Setbp1 Cdk6 Cxcr5 Fam20a Il1r1 Pim2 Gbp5 Ms4a4c Add3 H2-DMa Adh1 Sox4 Abcg3 Art2b Lypd6b Sntb1 Atp8b4 Tdrp
CD4+ T_EM cells
Stat1-/-
Stat3-/-
Upregulated
No change
Downregulated

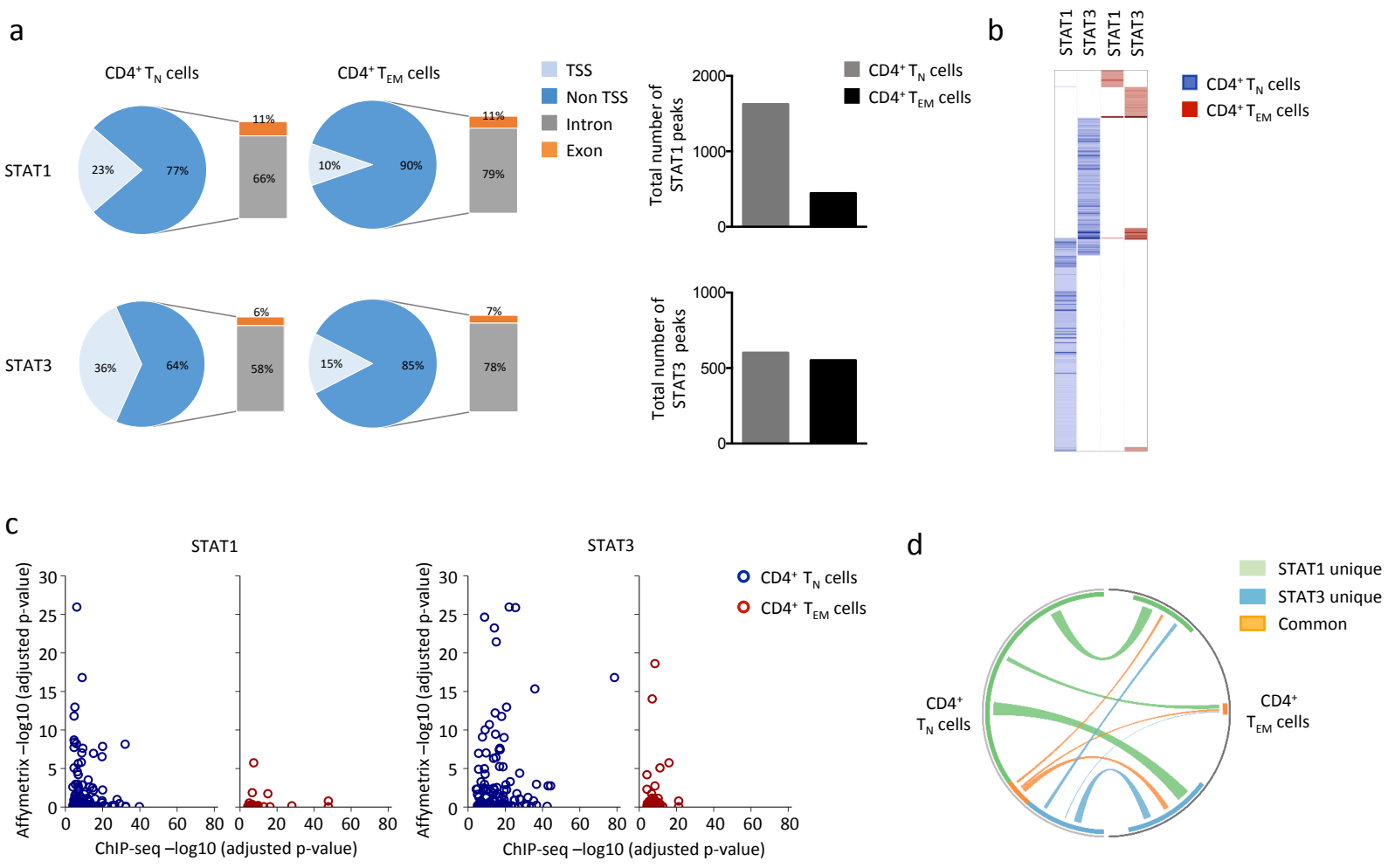
a
CD4+ TN cells
CD4+ TEM cells
STAT1
STAT3
23%
77%
11%
66%
10%
90%
11%
79%
36%
64%
6%
58%
15%
85%
7%
78%
TSS
Non TSS
Intron
Exon
Total number of STAT1 peaks
2000
1000
0
Total number of STAT3 peaks
1000
500
0
CD4+ TN cells
CD4+ TEM cells
b
STAT1
STAT3
STAT1
STAT3
CD4+ TN cells
CD4+ TEM cells
c
STAT1
STAT3
Affymetrix –log10 (adjusted p-value)
ChIP-seq –log10 (adjusted p-value)
0
5
10
15
20
25
30
0
20
40
60
80
CD4+ TN cells
CD4+ TEM cells
d
STAT1 unique
STAT3 unique
Common
CD4+ TN cells
CD4+ TEM cells

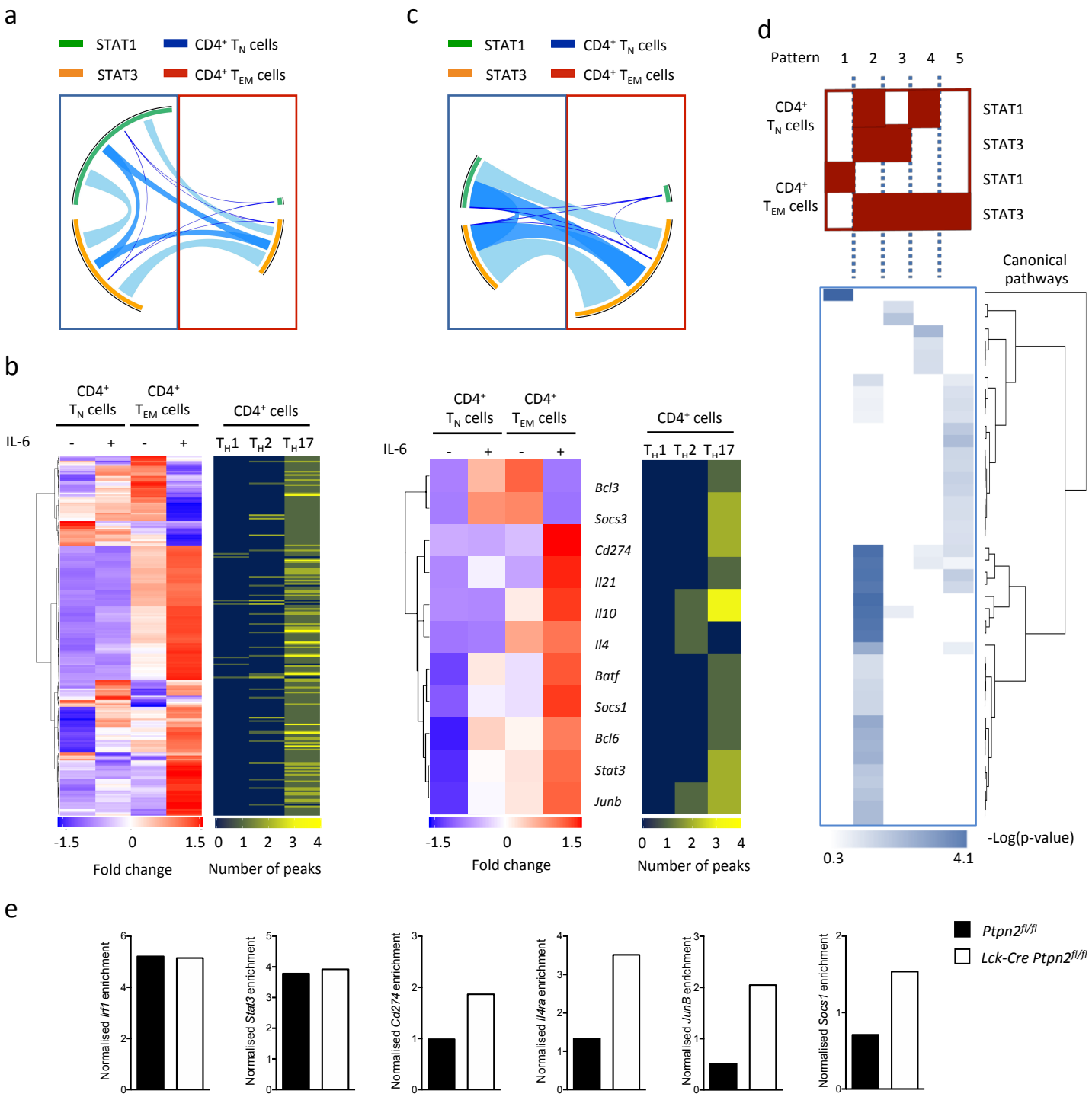
a
STAT1
STAT3
CD4+ TN cells
CD4+ TEM cells
c
STAT1
STAT3
CD4+ TN cells
CD4+ TEM cells
d
Pattern 1 2 3 4 5
CD4+ TN cells
CD4+ TEM cells
STAT1
STAT3
STAT1
STAT3
Canonical pathways
-Log(p-value)
0.3
4.1
b
CD4+ TN cells
CD4+ TEM cells
CD4+ cells
IL-6
- + - +
TH1 TH2 TH17
-1.5 0 1.5
Fold change
0 1 2 3 4
Number of peaks
Bcl3
Socs3
Cd274
Il21
Il10
Il4
Batf
Socs1
Bcl6
Stat3
Junb
e
Normalised Irf1 enrichment
Normalised Stat3 enrichment
Normalised Cd274 enrichment
Normalised Il4ra enrichment
Normalised JunB enrichment
Normalised Socs1 enrichment
Ptpn2fl/fl
Lck-Cre Ptpn2fl/fl

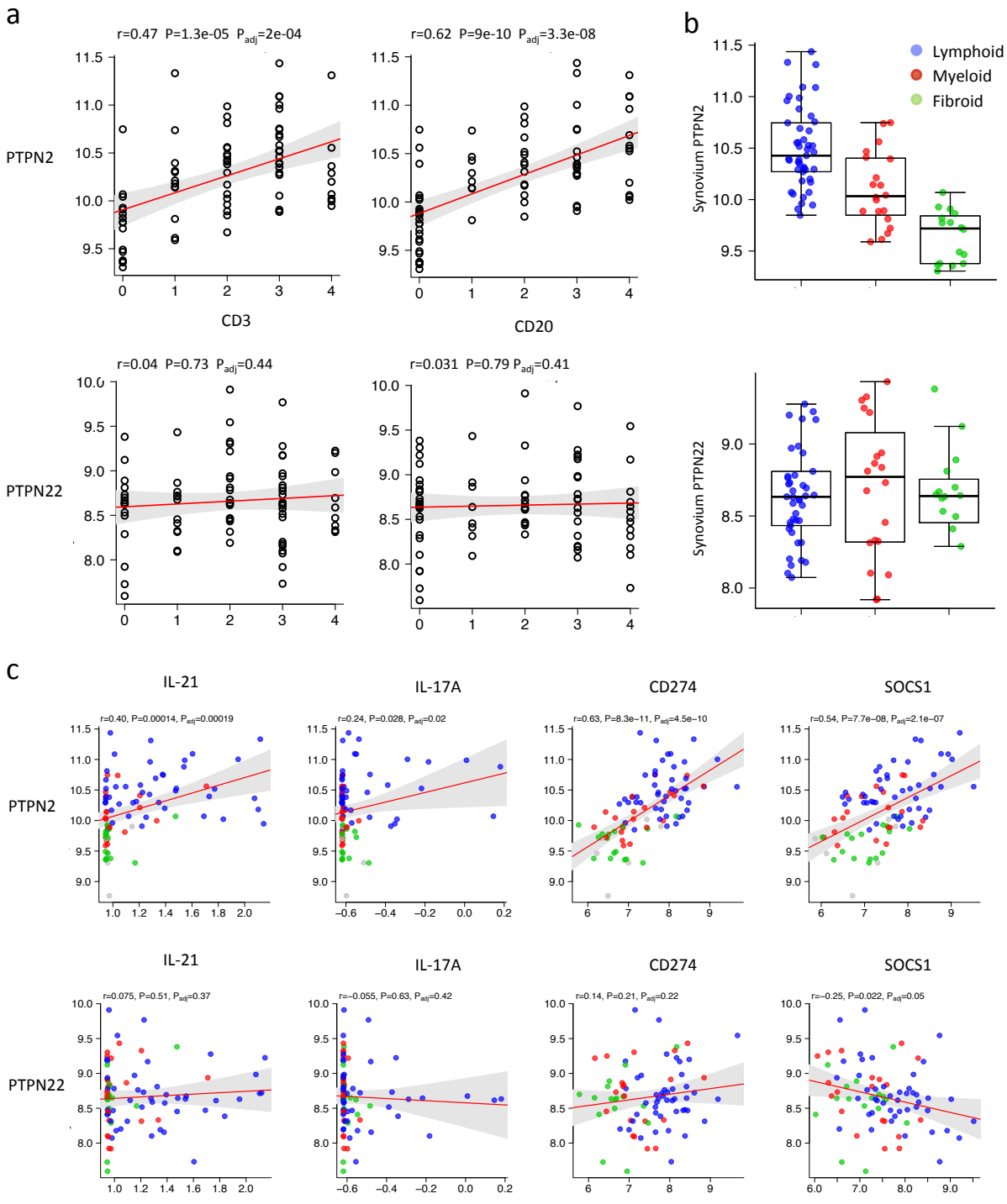
a
r=0.47 P=1.3e-05 P_adj=2e-04
r=0.62 P=9e-10 P_adj=3.3e-08
PTPN2
CD3
CD20
r=0.04 P=0.73 P_adj=0.44
r=0.031 P=0.79 P_adj=0.41
PTPN22
b
Lymphoid
Myeloid
Fibroid
Synovium PTPN2
Synovium PTPN22
c
IL-21
IL-17A
CD274
SOCS1
r=0.40, P=0.00014, P_adj=0.00019
r=0.24, P=0.028, P_adj=0.02
r=0.63, P=8.3e−11, P_adj=4.5e−10
r=0.54, P=7.7e−08, P_adj=2.1e−07
PTPN2
r=0.075, P=0.51, P_adj=0.37
r=−0.055, P=0.63, P_adj=0.42
r=0.14, P=0.21, P_adj=0.22
r=−0.25, P=0.022, P_adj=0.05
PTPN22